

Western  Graduate&PostdoctoralStudies

Western University  
Scholarship@Western

---

Electronic Thesis and Dissertation Repository

---

1-31-2013 12:00 AM

## pH Responsive Hydrogen Bonding Motif to Improve the Sensitivity of Tumor Imaging

Fatimah Mohammed Algarni  
*The University of Western Ontario*

Supervisor

Dr. James Wisner

*The University of Western Ontario* Joint Supervisor

Dr. Elizabeth Gillies

*The University of Western Ontario*

Graduate Program in Chemistry

A thesis submitted in partial fulfillment of the requirements for the degree in Master of Science

© Fatimah Mohammed Algarni 2013

Follow this and additional works at: <https://ir.lib.uwo.ca/etd>



Part of the [Nanoscience and Nanotechnology Commons](#), and the [Organic Chemistry Commons](#)

---

### Recommended Citation

Algarni, Fatimah Mohammed, "pH Responsive Hydrogen Bonding Motif to Improve the Sensitivity of Tumor Imaging" (2013). *Electronic Thesis and Dissertation Repository*. 1110.

<https://ir.lib.uwo.ca/etd/1110>

This Dissertation/Thesis is brought to you for free and open access by Scholarship@Western. It has been accepted for inclusion in Electronic Thesis and Dissertation Repository by an authorized administrator of Scholarship@Western. For more information, please contact [wlsadmin@uwo.ca](mailto:wlsadmin@uwo.ca).

**pH Responsive Hydrogen Bonding Motif to Improve the  
Sensitivity of Tumor Imaging.**

(Spine Title:) pH Responsive Motif to Improve Tumor Imaging.

(Thesis Format: Monograph)

By

**Fatimah M. Algarni**

**Graduate Program in Chemistry**

**Submitted in partial fulfillment  
of the requirements for the degree  
Master of Science**

**The School of Graduate and Postdoctoral Studies**

**University of Western Ontario**

**London, Ontario, Canada**

**January 2013**

**©Fatimah Algarni 2013**

THE UNIVERSITY OF WESTERN ONTARIO  
SCHOOL OF GRADUATE AND POSTDOCTORAL STUDIES

**CERTIFICATE OF EXAMINATION**

Supervisor

\_\_\_\_\_  
Dr. James Wisner  
Dr. Elizabeth Gillies

Supervisory Committee

\_\_\_\_\_  
Dr. Viktor Staroverov

Examiners

\_\_\_\_\_  
Dr. Len Luyt

\_\_\_\_\_  
Dr. Mel Usselman

\_\_\_\_\_  
Dr. Sohrab Rohani

The thesis by

**Fatimah M. Algarni**

entitled:

**pH Responsive Hydrogen Bonding Motif to Improve the Sensitivity of  
Tumour Imaging.**

is accepted in partial fulfillment of the  
requirements for the degree of  
Master of Science

Date \_\_\_\_\_

\_\_\_\_\_  
Chair of the Thesis Examination Board

## **Abstract**

Magnetic resonance imaging (MRI) is a powerful non-invasive medical diagnostic technique. Superparamagnetic iron oxide nanoparticles (SPIO) are effective contrast agents and provide high sensitivity contrast in MRI. Recent research has demonstrated that nanoparticle clusters exhibit significantly higher relaxivity than individual nanoparticles.

In order to increase the sensitivity of tumor imaging, supramolecular chemistry was introduced to this field and a novel conjugation method was developed using click chemistry between azide functionalized nanoparticles and pH-sensitive hydrogen bonding building blocks. This pH-sensitive hydrogen bonded complex was synthesized to cluster nanoparticles under mildly acidic biological conditions.

Due to the unexpected X-ray crystal structure of the acceptor molecule, erroneous results were obtained. An association constant ( $K_a$ ) was determined via  $^1\text{H}$  NMR titration of a similar hydrogen bonding system and the resulting value of  $194 \text{ M}^{-1}$  in DMSO. This result indicates the potential feasibility of this project. The synthesis, characterization, and tests of functionalized SPIO and monomers are reported.

## **Keywords**

MRI, SPIO, Contrast agent, Click chemistry, Hydrogen Bond, Supramolecular Polymer.

## **Acknowledgements**

First and foremost, I would like to thank my supervisors, Dr. James Wisner and Dr. Elizabeth Gillies, for providing me with an opportunity to pursue my master studies, and their guidance through the past two and a half years. I want to thank them for their constant support and guidance while undertaking this project. Their encouragement has caused me to strive to be a better student and scientist throughout my time here.

I would also like to thank all of the past and present Wisner's and Gillies' group members. I greatly appreciate my lab mates for providing a friendly atmosphere. Besides passing on the techniques.

I offer my regards to all of those (Secretaries in chemistry department, Staff in ChemBioStore, mass spectrometry, NMR, X-ray analysis) who supported me in any respect during my M.Sc. study and research.

Lastly, I would like to thank my family and friends in Saudi Arabia and Canada for their constant love and support. Last but not least, I thank God for giving me the determination and strength to pursue my goals.

# Table of Contents

	Page
CERTIFICATE OF EXAMINATION	ii
ABSTRACT	iii
ACKNOWLEDGEMENTS	iv
TABLE OF CONTENTS	v
LIST OF SCHEMES	vii
LIST OF FIGURES	viii
LIST OF ABBREVIATIONS	x
Chapter 1: Introduction	1
1.1 Supramolecular Polymers	3
1.1.1 Hydrogen bonding in supramolecular chemistry	3
1.1.2 Factors affecting the strength of hydrogen bonding	4
1.1.2.1 Numbers of Hydrogen Bonds	4
1.1.2.2 Secondary interactions	5
1.1.2.3 Acidity and basicity of the donor and acceptor	8
1.1.2.4 Solvents	10
1.2 Magnetic Resonance Imaging	13
1.2.1 MRI and Tumour imaging	13
1.2.2 MRI Principles	13
1.2.3 Paramagnetic Contrast Agents	15
1.2.4 Superparamagnetic iron oxide nanoparticles (SPIO) as contrast agents	13

1.2.5 Targeted iron oxide nanoparticles	16
1.3 The Proposal	18
1.3.1 The design	20
Chapter 2: Results and Discussion	22
2.1. Synthesis	23
2.1.1 Synthesis of Donor Molecule	23
2.1.2 Synthesis of Acceptor Molecule.	25
2.1.3 Synthesis of Dextran Coated SPIO	29
2.1.4 Synthesis of the linker	31
2.1.5 Conjugating Donor and Acceptor to Nanoparticles	32
2.1.6 Synthesis of Donor and Acceptor Monomers	36
2.2. pK <sub>a</sub> Titrations	38
2.3. The Affect of Changing pH on the Aggregation of the Nanoparticles	41
2.4. X-ray crystallography	42
2.5. <sup>1</sup> H NMR Titration	44
Chapter 3: Conclusions and Future Work	45
Chapter 4: Experimental	48
4.1 General Procedures and Materials	49
4.2 Experimental Section	50
Chapter 5: References	66
Curriculum Vitae	71

## List of Schemes

<b>Scheme 1:</b> Hydrogen bonding between two electronegative atoms D and A mediated by a hydrogen atom, H.	3
<b>Scheme 2:</b> Synthesis of the donor molecule.	23
<b>Scheme 3:</b> Synthesis of <b>6</b> .	25
<b>Scheme 4:</b> Synthesis of <b>8</b> .	26
<b>Scheme 5:</b> Synthesis of <b>12</b> .	26
<b>Scheme 6:</b> Synthesis of <b>13</b> .	27
<b>Scheme 7:</b> Synthesis of the acceptor molecule, <b>14</b> .	28
<b>Scheme 8:</b> Synthesis of dextran-coated Fe <sub>3</sub> O <sub>4</sub> nanoparticles.	29
<b>Scheme 9:</b> Synthesis of the linker.	31
<b>Scheme 10:</b> Synthesis of the functionalized nanoparticles.	32
<b>Scheme 11:</b> Synthesis of the PEG derivative.	36
<b>Scheme 12:</b> Synthesis of the donor, <b>26</b> and Acceptor, <b>27</b> monomers.	37
<b>Scheme 13:</b> synthesizing 2,6-diaminopyridin-1-ium chloride.	38
<b>Scheme 14:</b> synthesis of the acceptor	43
<b>Scheme 15:</b> suggested future work	47



## List of Figures

<b>Figure 1:</b> increasing the $K_a$ value with an increase of the number of hydrogen bonds.	5
<b>Figure 2:</b> Secondary interactions based on the sequences of donors and acceptors in triply hydrogen bonded complexes.	6
<b>Figure 3:</b> $K_a$ values of triply hydrogen-bonded complexes in $CDCl_3$ .	6
<b>Figure 4:</b> an AAAA–DDDD quadruple hydrogen-bond complex.	7
<b>Figure 5:</b> the effect of substituents on the association constant.	8
<b>Figure 6:</b> the effect of charges on the association constant.	9
<b>Figure 7:</b> The intended 2:1 donor: acceptor complex and the resulting 1:1 complex observed in the solid state.	12
<b>Figure 8:</b> The x-ray crystal structure of the 1:1 complex. Primary hydrogen bonds and $\pi$ - $\pi$ stacking interactions are evident in the structure.	12
<b>Figure 9:</b> positive contrast agents and negative contrast agents images of coronal brain slices of mice infected with <i>T. gondii</i> .	15
<b>Figure 10:</b> The primary and secondary interactions that are expected for the target complex.	18
<b>Figure 11:</b> clicking donor and acceptor molecules to SPIO nanoparticles.	20
<b>Figure 12:</b> clicking donor and acceptor molecules to a bifunctional monomer.	21
<b>Figure 13:</b> Size distribution of nanoparticles <b>15</b> and <b>16</b>	30
<b>Figure 14:</b> UV-Vis absorbance of nanoparticles <b>15</b> and <b>16</b>	30
<b>Figure 15:</b> UV-Vis absorbance of nanoparticles <b>16</b> in pH 7.4 aqueous buffer and <b>21</b>	33
<b>Figure 16:</b> Size distribution of nanoparticles <b>21</b> .	34
<b>Figure 17:</b> Infrared spectra illustrating changes on nanoparticle surface.	34
<b>Figure 18:</b> Size distribution of nanoparticles <b>22</b> and <b>23</b>	35
<b>Figure 19:</b> Weak acid-strong base titration of 2,6-diaminopyridinium chloride.	39
<b>Figure 20:</b> Weak acid-strong base titration of <b>26</b> HCl salt.	40
<b>Figure 21:</b> Z-average size changing with pH.	41

**Figure 22:** X-ray crystal structure of **14**. 42

**Figure 23:** Titration curves for complex **G**. 44

## List of Abbreviations

A	acceptor
AT	adenine-thymine
°C	degrees celsius
CG	cytosine-guanine
$\delta$	chemical shift
D	donor
DCC	dicyclohexylcarbodiimide
DLS	dynamic light scattering
DMF	N,N-dimethylformamide
DMF	dimethylformamide
DMSO	dimethylsulfoxide
DNA	deoxyribonucleic acid
ESI	electrospray ionization
EDTA	ethylenediaminetetraacetic acid
g	gram
$\Delta G$	change in Gibbs free energy
h	hour
Hz	hertz
IR	infrared spectroscopy
$K_a$	association constant
kJ	kilo Joule
m	multiplet
$M^{-1}$	$(\text{mol/liter})^{-1}$
mCPBA	metachloroperoxybenzoic acid

min	minute
mL	milliliter
mmol	millimole
mol <sup>-1</sup>	/mol
m.p.	melting point
MRI	magnetic resonance imaging
MWCO	molecular weight cutoff
NMR	nuclear magnetic resonance
RF	radio frequency
SPIO	superparamagnetic iron oxides
TBAF	tetrabutylammonium fluoride
THF	tetrahydrofuran
TMSA	trimethylsilylacetylene

# **Chapter 1: Introduction**

The hydrogen bonding and  $\pi$  stacking interactions between natural complementary DNA nucleobases, adenine-thymine (A-T) and guanine-cytosine (G-C), are responsible for the stabilization of the double helical DNA structure and contribute to its central biological processes of transcription and replication. These examples provide an inspiration to use heteroaromatic building blocks to build molecules that can interact through hydrogen bonding and  $\pi$ - $\pi$  stacking to self-assemble and form new non-traditional *supramolecular* polymers.<sup>1</sup>

Unlike classical polymers where individual building blocks are connected by covalent bonds, supramolecular polymers are held together by non-covalent interactions. These non-covalent bonds are weaker than covalent bonds and reversible, which give supramolecular polymers switchable properties. As a result, supramolecular polymers are affected by their surrounding environment such as temperature, polarity of the solvent, or pH.<sup>2,3</sup>

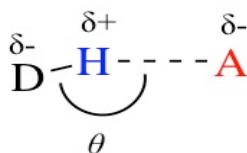
Inspired by a pH switchable supramolecular polymer, the idea of using such a system to signal the presence of tumours due to differences in pH between normal and cancerous tissues have been brought to light.<sup>3</sup> Thus, the design of a recognition system that capitalizes on pH dependent recognition could be used to increase the sensitivity of tumor imaging. Herein, we describe the elaboration of a pH dependent recognition motif that may be combined with iron oxide nanoparticles and used as contrast agent in magnetic resonance imaging (MRI) in an attempt to improve the sensitivity of tumour imaging.

## 1.1 Supramolecular Polymers

The non-covalent interactions between building blocks of supramolecular polymers such as electrostatic interactions, coordination bonds, hydrogen bonding,  $\pi$ - $\pi$  interactions, van der Waals forces and hydrophobic effects are the key to control the supramolecular polymer formation through molecular recognition and self-organization.

### 1.1.1 Hydrogen bonding in supramolecular chemistry

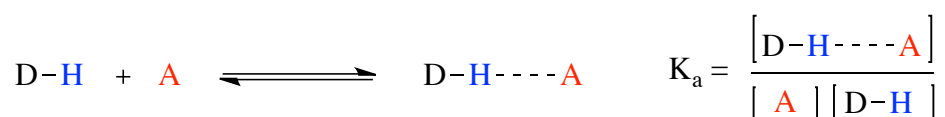
A hydrogen bond is an interaction between a hydrogen atom (donor) and an electronegative atom, such as nitrogen or oxygen (acceptor). The hydrogen atom is usually covalently bonded to another more electronegative atom such as O, N, S, F, Cl, Br or I causing the hydrogen atom to obtain a significant amount of positive charge. The strength of the hydrogen bond is dependent on the dipole moment of the donor, the negative charge on the acceptor and the angle of interaction. The strength of hydrogen bonds is usually in the range of 20 - 25 kJ/mol, but it can reach as high as 160 kJ/mol in  $F-H\cdots F^-$ . Typically three atoms (D-H $\cdots$ A) are arranged with an ideal angle ( $\theta$ ) close to 180°.



**Scheme 1:** Hydrogen bonding between two electronegative atoms D and A mediated by a hydrogen atom, H.

### 1.1.2 Factors affecting the strength of hydrogen bonding

The hydrogen bonding strength and stability in these self-assembled molecules depends on many factors such as numbers of hydrogen bonds, secondary interactions, the acidity of the donors and the basicity of the acceptor atoms and solvents. The measurement of the binding strength is called the association constant ( $K_a$ ), which is the mathematical constant that describes the affinity of two molecules at equilibrium:



#### 1.1.2.1 Numbers of Hydrogen Bonds

A positive relationship is observed between the number of hydrogen bonds and the stability of resulting complexes (Figure 1).<sup>4</sup> The increase in stability is due to the increase of the binding energy that is based on the increase of the number of hydrogen bonds. This relationship is observed in the differences in the association constant between the G-C base pair and the A-T base pair. Since the G-C base pair has three hydrogen bonds while the A-T base pair has two hydrogen bonds, the association constant and the stability of the G-C base pair ( $K_a = 10^4$ - $10^5 \text{ M}^{-1}$  in  $\text{CDCl}_3$ ) is greater than the A-T base pair ( $K_a = 10^2 \text{ M}^{-1}$  in  $\text{CDCl}_3$ ).<sup>5</sup> Based on this observation, a complex consisting of four hydrogen bonds will have a higher association constant than the DNA base pairs. A  $K_a$  value of  $3 \times 10^7 \text{ M}^{-1}$  was measured for a DAAD.ADDA complex that Zimmerman and coworkers synthesized.<sup>1</sup>



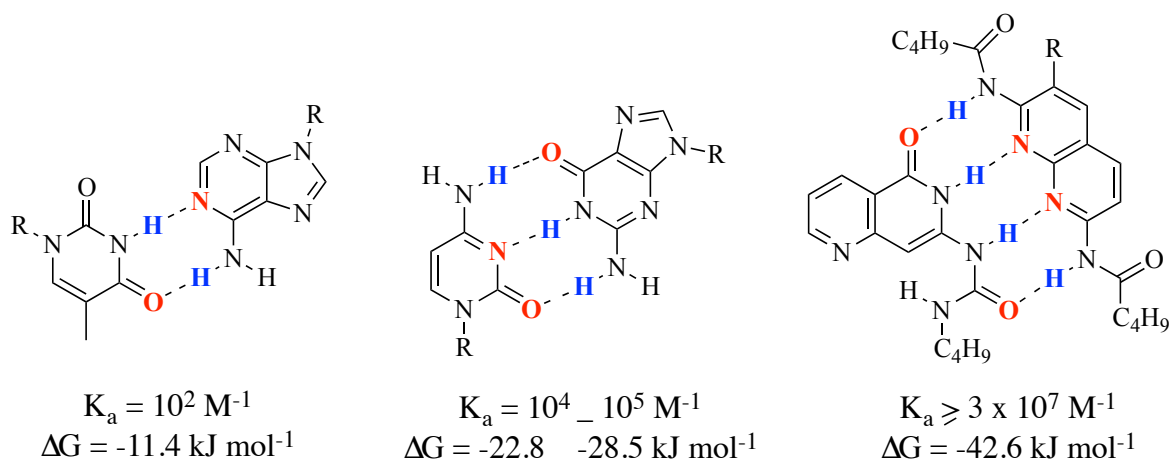


**Figure 1:** Increasing  $K_a$  value with an increase in the number of hydrogen bonds.

### 1.1.2.2 Secondary interactions

The stability of a complex may be determined not only by the number of hydrogen bonds, but also the arrangement of the hydrogen bond donor and acceptor sites in the two molecules forming the complex (Figure 2). In 1990, a study was performed by Jorgenson and Pranata to illustrate the effect of the secondary interactions in DNA-like triply hydrogen bonded complexes. They found that the strength and the stability of the complexes have a positive relationship with the number of attractive secondary electrostatic interaction between donors and acceptors atoms and an inverse relationship with secondary repulsion between them.<sup>1,6</sup> As a result, an AAA-DDD complex will have more stability and strength than an ADA-DAD or an AAD-DDA complex because it has another two-four attractive secondary hydrogen bonds beside the primary hydrogen bonds and no repulsive secondary interactions.

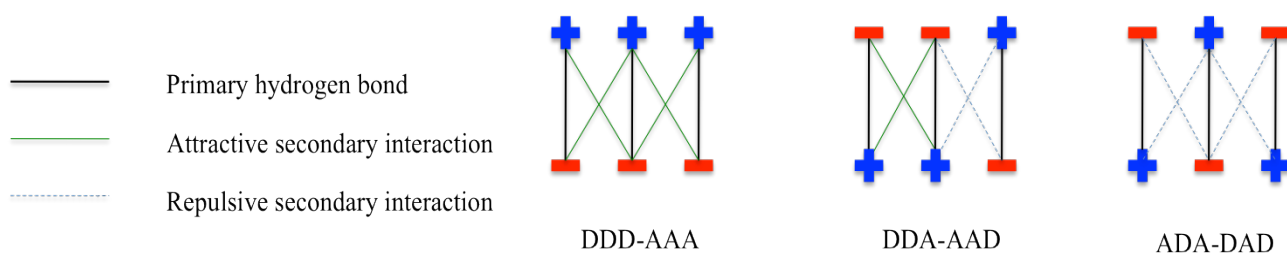


**Figure 2:** Secondary interactions based on the sequences of donors and acceptors in triply hydrogen bonded complexes.

For example, complex **A** has a  $K_a$  value  $>10^5 \text{ M}^{-1}$  in  $\text{CDCl}_3$  (Figure 3).<sup>7</sup> In comparison, the AAD-DDA complex has two attractive secondary hydrogen bonds and two repulsive secondary interactions and because of that it has a lower  $K_a$  value than complex **B** ( $K_a = 10^4\text{-}10^5 \text{ M}^{-1}$ ).<sup>6</sup> Finally, the ADA-DAD complex with four repulsive secondary interactions has the lowest  $K_a$  value for triply hydrogen bonded complexes (complex **C** with  $K_a = 78 \text{ M}^{-1}$ ).<sup>1</sup>

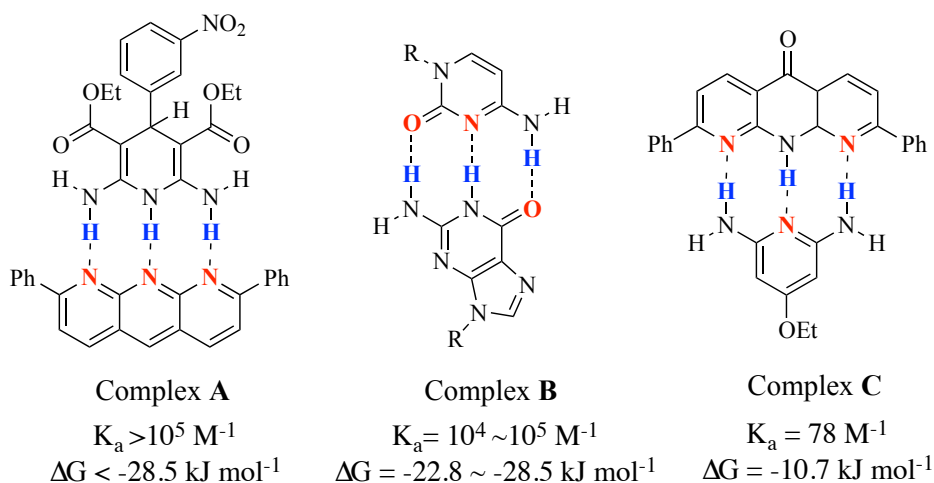
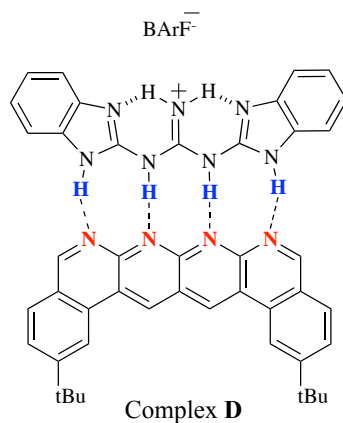


**Figure 3:**  $K_a$  values of triply hydrogen-bonded complexes in  $\text{CDCl}_3$ .

In 2011, Leigh and coworkers combined the effect of both hydrogen bond number and the secondary interactions to synthesize complex **D**, which contains an AAAA–DDDD quadruple hydrogen-bond complex that has an extremely high  $K_a$  value in non-polar solvents (Figure 4).<sup>8</sup>



$$K_a > 3 \times 10^{12} \text{ M}^{-1}, \Delta G = -71.1 \text{ kJ mol}^{-1} \text{ in CH}_2\text{Cl}_2$$
$$K_a = 1.5 \times 10^6 \text{ M}^{-1}, \Delta G = -35.2 \text{ kJ mol}^{-1} \text{ in CH}_3\text{CN}$$
$$K_a = 3.4 \times 10^5 \text{ M}^{-1}, \Delta G = -31.5 \text{ kJ mol}^{-1} \text{ in 10\% v/v DMSO/CHCl}_3$$

**Figure 4:** an AAAA–DDDD quadruple hydrogen-bond complex.

### 1.1.2.3 Acidity and basicity of the donor and acceptor

The individual or primary hydrogen bond strength is affected by the acidity of the donor and basicity of the acceptor. Applying that to a multiple hydrogen bonding complex, we can determine the strength and stability based on the expecting the pKa values and altering it by changing the functional groups on the complex.<sup>1</sup> In 1966, Yoshimasa and coworkers investigated the effect of substituents of the hydrogen bonding of adenine and uracil derivatives on the association constants of their complexes (Figure 5). Their study indicated the role substituents might play to enhance or decrease the strength of the adenine-uracil association.

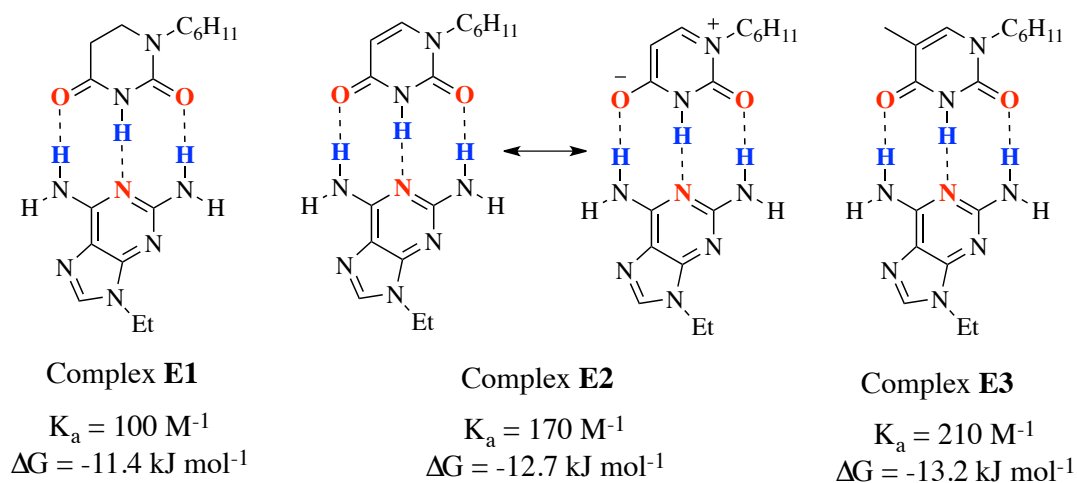
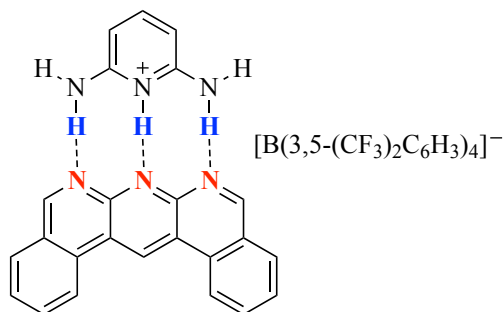


**Figure 5:** The effect of substituents on the association constant.

First, the loss of aromaticity because of the hydrogenation in 5,6-dihydrouracil is responsible for the increase of the K<sub>a</sub> value in complex E2 than E1. The resonance in

complex **E2** gives the 4-carbonyl oxygen atom more electron density and more basicity as a result. In addition, the  $pK_a$  of the amide group increased from 9.4 in uracil to 11 or larger in **E2**. Secondly, adding a methyl group to uracil in complex **E3** increased the association complex. This increase is due to the role of the methyl group as an electron donor which increased further the basicity of the 4-carbonyl oxygen and increased the  $pK_a$  value of the amide group from 9.4 to 9.9.<sup>9</sup>

Moreover, having appropriate charge in the complex will increase stability.<sup>1</sup> We can see the huge increase in strength that a complex gains from the  $K_a$  value of complex **F**, ( $K_a = 3 \times 10^{10} \text{ M}^{-1}$  in  $\text{CH}_2\text{Cl}_2$ ) because the positive charge in the cationic DDD enhances the hydrogen bond donor character and gives electrostatic stabilization to the complex.<sup>10</sup>



**Complex F**  
 $K_a = 3 \times 10^{10} \text{ M}^{-1}$   
 $\Delta G = -59.7 \text{ kJ mol}^{-1}$

**Figure 6:** the effect of charge on the association constant.

#### 1.1.2.4 Solvents

Another important factor that affects the strength and stability of hydrogen bonded complexes is the solvent. Generally, there is an inverse relationship between solvent polarity and hydrogen bonding strength. Less polar solvents such as hydrocarbons increase the strength while protic or polar solvents such as water or DMSO decrease it.<sup>1</sup> Therefore most hydrogen bonded supramolecular complexes are characterized in chloroform or toluene, but unfortunately the solubilities of some donors or acceptors are poor in these solvents and this can cause complications. In 2007, Hunter and his coworkers studied the effects of different solvents on the association constants for formation of a 1:1 complex between tri-*n*-butylphosphine oxide and perfluoro-*tert*-butyl alcohol at 295 K. The results in the table below illustrates the higher association constants in CCl<sub>4</sub> and cyclohexane over DMSO and other polar solvents due to lack of competition with the hydrogen bonds of the complex.<sup>11</sup>

Solvents	Association constants ( $K_a$ in $M^{-1}$ )
DMSO	$6.8 \times 10^{-1}$
Acetone	$6.5 \times 10^{-1}$
Acetonitrile	$1.6 \times 10^2$
Tetrahydrofuran	$2.4 \times 10^2$
CHCl <sub>3</sub>	$2.7 \times 10^3$
CCl <sub>4</sub>	$7.6 \times 10^4$
Cyclohexane	$>10^5$

In another study, Rehm and Schmuck reported many solutions to increase the strength of self-assembly in polar solvents based on previous research and their own research because most hydrogen bond assemblies are not stable enough to be useful in polar protic solvents on their own.<sup>2</sup> First, using strong metal–ligand interactions in addition to hydrogen bonds gives the hydrogen bond-mediated assembly stability in water because a coordination bond between the metal and the ligand can be as stable as a covalent bond. On the other hand, this technique can have disadvantages such as toxicity and high cost. Ion-pair formation is the second solution because the electrostatic interaction is more stable than hydrogen bonding but not as much as the coordinate bond in metal–ligand interaction and this charge interaction beside hydrogen bonding is very important for the stability of a self-assembly in polar protic solvents. Finally, adding functional groups that have an additional electron-donor or acceptor to the monomer contributes with the other methods to form a stable and strong self-assembly in polar protic solvents.<sup>2</sup>

However, these solutions may still not work in polar protic solvents if we employ only individual complexes. Multivalency of many of the same groups on the surface of a nanoparticle will also contribute to the stability of an aggregate by increasing the number of recognition events.

In recent work performed in the Wisner group, a complex between 2,6-diaminopyridinium tetraphenylborate and 1,2-bis(5,7-dimethyl-1,8-naphthyridin-2-yl)diazene was synthesized. The original intention was a 2:1 complex where the acceptor molecule binds to two triple donor molecules (Figure 7, left). However, after obtaining the X-ray crystal structure, they found that one of the naphthyridine rings flipped over

and formed a 1:1 complex with four primary hydrogen bonds (Figure 7, right).

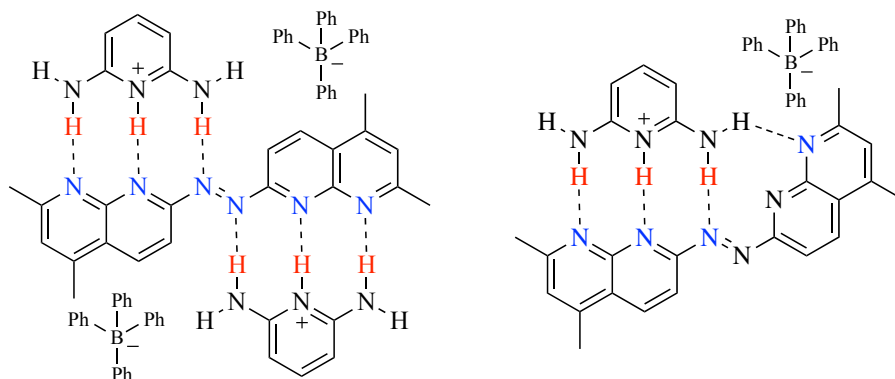


**Figure 7:** The intended 2:1 donor: acceptor complex (left) and the resulting 1:1 complex (right) observed in the solid state.

The crystal was obtained from acetonitrile and isopropyl ether, and there are four primary hydrogen bonds. In addition, there are  $\pi$ - $\pi$  stacking interactions between the planar complexes (Figure 8).<sup>12</sup> Based on the previously reported complex F, and because of the extra hydrogen bond this complex should have  $K_a \gg 3 \times 10^{10} \text{ M}^{-1}$  in chlorinated solvents.

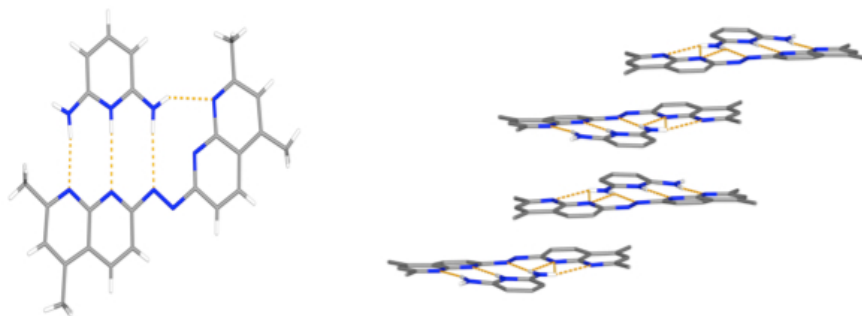


**Figure 8:** The x-ray crystal structure of the 1:1 complex.<sup>12</sup> Primary hydrogen bonds (left) and  $\pi$ - $\pi$  stacking interactions (right) are evident in the structure.



## **1.2 Magnetic Resonance Imaging (MRI)**

### **1.2.1 MRI and Tumour imaging**

In another important field, scientists continually attempt to find the best techniques for clinical diagnosis in order to help them differentiate between normal and diseased tissue without having to perform surgery to elucidate a patient's illness. Since the invention of Magnetic Resonance Imaging (MRI), many contrast agents have been used to change the relaxation times of protons in water molecules in order to better distinguish between normal and diseased tissue. MRI has been used for cancer imaging for many years,<sup>13</sup> as cancer is one of the leading causes of death. While most previously developed contrast agents distinguish tumors from normal tissue on the basis of their leaky vasculature, there is a potential for tumor imaging based on the fact that differences in pH exist between normal tissues and the blood stream which are around 7-7.4 and between tumors which are more acidic where the pH can reach 6 in the extracellular core of the tumor.<sup>14</sup>

### **1.2.2. MRI Principles**

The principles of MRI are similar to those of Nuclear Magnetic Resonance (NMR) spectroscopy and depend on the density of protons in the targeted area and the degree of polarization of the nuclear spin states.<sup>15</sup> When placed in a strong magnetic field ( $B_0$ ), proton nuclei, which have a non-zero magnetic moment, will orient either anti-parallel (high energy state) with the main magnetic field ( $B_0$ ) or parallel (low energy state) with a slight majority reaching a thermal equilibrium, and a precessional motion about  $B_0$  at some frequency. This slight excess of spins in the low energy state will form a net magnetization aligned parallel with  $B_0$ . A radiofrequency (RF) coil has two important

jobs in MRI. First, excitement of the proton nuclei occurs in response to a radiofrequency (RF) pulse from this coil, which creates a new magnetic field ( $B_1$ ). The RF pulse affects the orientation of the proton nuclei, causing tipping of the overall net magnetization toward the transverse plane, which is perpendicular to the main magnetic field ( $B_0$ ). This tipping is due to transition of some spins from the low energy state to high energy state after absorbing energy from the RF. Also, the spins become phase coherent in the transverse plane. In order to begin detecting MR signals, the RF pulse will be turned off allowing nuclei to return into their original states (before performing a radiofrequency (RF) pulse). These MR signals that are caused from the oscillation of the protons translate into electrical current in the same radiofrequency (RF) coil creating the MR signal.<sup>16</sup>

There are two relaxation mechanisms depending on how the nuclei return to their original states.  $T_1$  and  $T_2$  are relaxation times corresponding to longitudinal and transverse relaxation mechanisms.  $T_1$  is defined by the time that a radiofrequency excited proton in ( $B_1$ ) magnetic field takes to return to the main magnetic field ( $B_0$ ) or to the longitudinal axis after turning off the RF pulse.  $T_2$  corresponds to the decay of the proton around the transverse axis ( $B_0$ ) after losing phase coherence.<sup>15</sup> The differences in water concentration and environment between healthy and diseased tissues give inherent differences in  $T_1$  and  $T_2$  relaxation times. For example, since the water concentration is higher in cancerous tissue than the normal tissue, the  $T_2$  values for them are different, 0.043 seconds for normal and 0.056 seconds for cancerous tissue, and they exhibit different  $T_1$  values as well.<sup>16</sup>

### 1.2.3. Paramagnetic Contrast Agents

The using of paramagnetic contrast agents has rendered MRI one of the most important medical imaging techniques currently developed because of the advantages of these paramagnetic contrast agents comparing to those for other imaging modalities. For example, they do not emit ionizing radiation. They are not visualized directly but rather affect the relaxation of water and fat protons in their surrounding areas.<sup>17</sup> There are two main types of paramagnetic contrast agents that are clinically used based on their effect on  $T_1$  or  $T_2$  relaxation times. First, gadolinium contrast agents affect  $T_1$  relaxation times more strongly and are called positive contrast agents because they lead to increases in the MRI signal intensity under most pulse sequences. Second, superparamagnetic iron oxide nanoparticles alter  $T_2$  relaxation times more strongly and they are called negative contrast agents. They lead to decreases in the MRI signal intensity, often called signal voids in their vicinity.

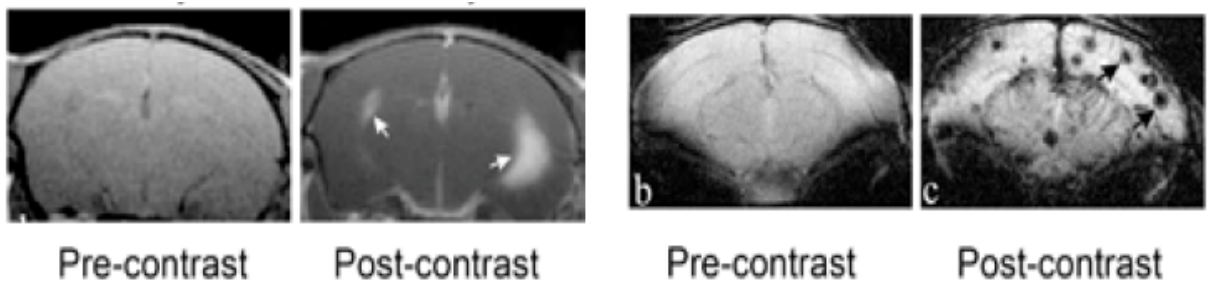


**Figure 9:** Positive contrast agents (left two images) and negative contrast agents (right two images) images of coronal brain slices of mice infected with *T. gondii*.<sup>18</sup>

#### **1.2.4 Superparamagnetic iron oxide nanoparticles (SPIO) as contrast agents**

The emergence of superparamagnetic iron oxide nanoparticles was very important to avoid some disadvantages such as short retention time *in vivo*, toxicity and biocompatibility of other contrast agents like gadolinium.<sup>13</sup> Another advantage of iron oxide nanoparticles is their sensitivity and they present inhomogeneities in the magnetic field causing a decrease in  $T_2$  relaxation times of healthy tissue. This decrease generates a big difference in  $T_2$  relaxation time between normal and diseased tissues and, as a result, the differences in the signal between them.<sup>16,19</sup> In order to allow these nanoparticles to work in cells, iron oxide nanoparticles are coated by water soluble polymers such as dextran to render them soluble in aqueous or biological media and also to make a colloidal suspension more stable.<sup>20</sup> Iron oxide nanoparticles were functionalized with azide groups and further derivatized using click chemistry.<sup>19</sup> This method facilitates the conjugation of the nanoparticles to any active targeting group for many applications in MRI.

#### **1.5 Targeted iron oxide nanoparticles**

One of the important uses of the iron oxide nanoparticles is targeting specific areas in the body by taking advantage of *in vivo* macrophages or attaching specific targeting groups to the surface of the nanoparticle. First of all, iron oxide nanoparticles can be used to image the liver and spleen due the natural uptake of the nanoparticles by macrophages, which work as non-specific defenses against any foreign material.<sup>21</sup> Despite the benefit of macrophages in imaging, it makes it difficult to image any other areas in the body. Thus, attaching specific targeting groups on the surface of the

nanoparticles is a highly desirable goal. The size of the nanoparticles should be less than 100 nm to increase the prolonged circulation in the blood stream and avoid non-specific uptake by macrophages. There are many examples of attaching peptides, antibodies and small molecules to the surface of nanoparticles. As an example of attaching peptides, in 2005, glioma brain tumors were detectable by both MRI and fluorescence imaging. This detection was enabled by attaching chlorotoxin and Cy5.5 to coated iron oxide nanoparticles with covalently bound bifunctional poly(ethylene glycol) (PEG). Chlorotoxin peptide has a high affinity for the membrane-bound matrix metalloproteinase-2 endopeptidases that are found in gliomas, medulloblastomas, the neuroectodermal origin tumors.<sup>22</sup> Secondly, in the area of using antibodies, having a prostate-specific membrane antigen mostly on the neovasculature of solid tumors and on the surface of prostate cells helped to develop biotinylated anti-PSMA iron oxide nanoparticles that improve the magnetic resonance detection of prostate cancer cells.<sup>23</sup> Finally, folic acid was conjugated to superparamagnetic iron oxide nanoparticles coated by covalently bound bifunctional PEG. It is known that the folate receptor is overexpressed on the surfaces of many human tumor cells such as ovarian, lung, breast, endometrial, renal, and colon cancers. This conjugation of folic acid on the nanoparticles results in a significant uptake by target cells in comparison with nanoparticles coated with PEG or dextran alone.<sup>24</sup> Thus, in order to target specific areas for *in vivo* imaging, attaching active targeting groups on the surface of SPIO is essential to achieve this goal.

### 1.3 The Proposal

This project combines the two described important fields above. It involves the synthesis of a pH-sensitive hydrogen bonded complex and its attachment to iron oxide nanoparticles by click chemistry in order to increase the sensitivity of these nanoparticles for tumor imaging. This increased sensitivity will be achieved because the hydrogen bonding moieties will be designed to assemble selectively at the mildly acidic pH of tumor tissue. This bonding is anticipated to induce clustering of the nanoparticles. It has been previously demonstrated that nanoparticle clusters exhibit significantly higher relaxivity than individual nanoparticles.<sup>25</sup> Therefore, the ability to detect the tumor will be enhanced by this selective clustering in tumor tissue. Based on the requirement for hydrogen bonding induced by mildly acidic pH and previous reports on hydrogen bonding moieties,<sup>10,12</sup> the monomers were chosen (Figure 10). The hydrogen bonding monomers are 3-ethynylpyridine-2,6-diamine (donor molecule) and (E)-7-((5-ethynylpyridin-2-yl)diazenyl)-2-(2-(2-(2-methoxyethoxy)ethoxy)ethoxy)-4-methyl-1,8-naphthyridine (acceptor molecule).

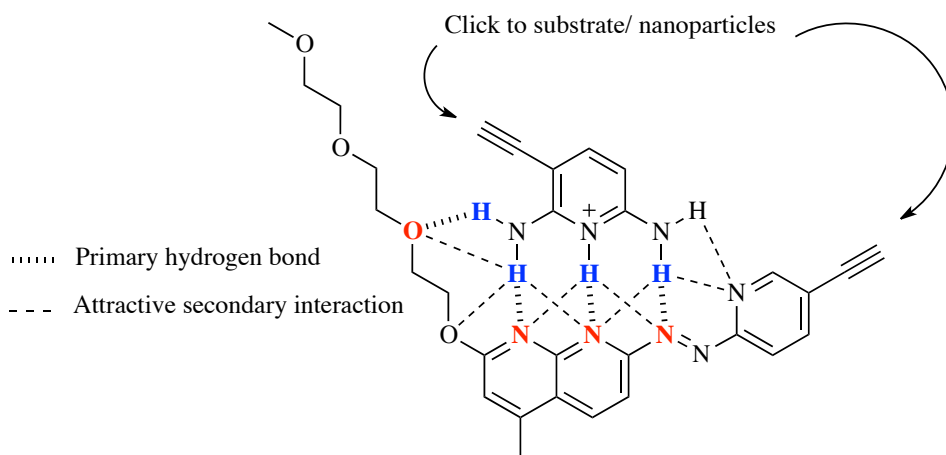
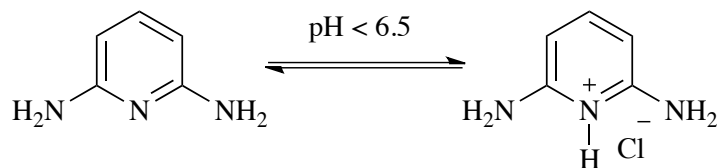


**Figure 10:** The primary and secondary interactions that are expected for the target complex.

The  $pK_a$  value of the donor molecule was measured by weak acid-strong base titration and it was found to be 6.5.



This value means that under pH 6.5 there will be more protonated molecule, 2,6-diamino-3-ethynylpyridin-1-ium than 3-ethynylpyridine-2,6-diamine. The formation of this cation and having more of it within this region should enhance assembly by hydrogen bonding and  $\pi$ - $\pi$  stacking. The design of the pH-sensitive hydrogen bonded complex takes into account some of the factors that can help to make it a strong and stable complex and that will work in polar protic solvents such as water. First, the sequences of donors and acceptors is an AAAA-DDDD arrangement, so it increases the number of attractive secondary electrostatic interactions between donor and acceptor atoms and eliminates any repulsive interaction between them. Second, using a hydrophilic group (triethylene glycol) in the acceptor molecule improves its water solubility. Also, adding functional groups that have electron-acceptors (oxygen atoms) to the acceptor molecule increases the number of the hydrogen bonds in the complex in order to form a stable self-assembly in polar protic solvents.

### 1.3.1 The design

The design of this project has two main lines of inquiry. First, the donor and the acceptor molecules are going to be attached to the iron oxide nanoparticles by click chemistry between the alkyne group in the hydrogen bonding molecules and the azide group in the nanoparticles, separately and then mix them together (Figure 11) and their behavior will be observed with respect to aggregation in response to pH changes.

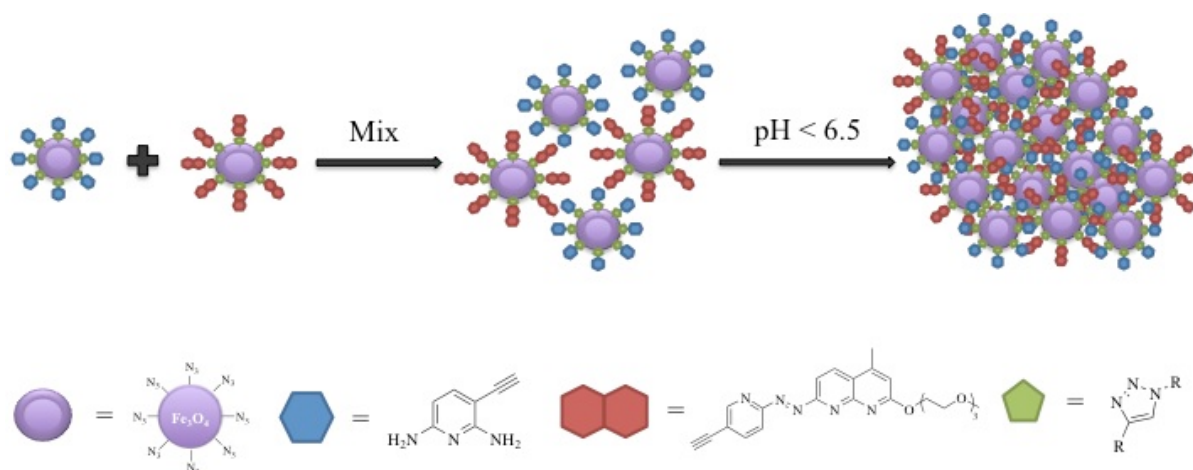


**Figure 11:** clicking donor and acceptor molecules to SPIO nanoparticles.

Second, the donor and the acceptor molecules are going to be attached to bifunctional monomers by click chemistry, between the alkyne group in the hydrogen bonding molecules and the azide groups in a bifunctional monomer, separately and then mix them together (Figure 12) and their behavior will be observed with respect to aggregation in response to pH changes.



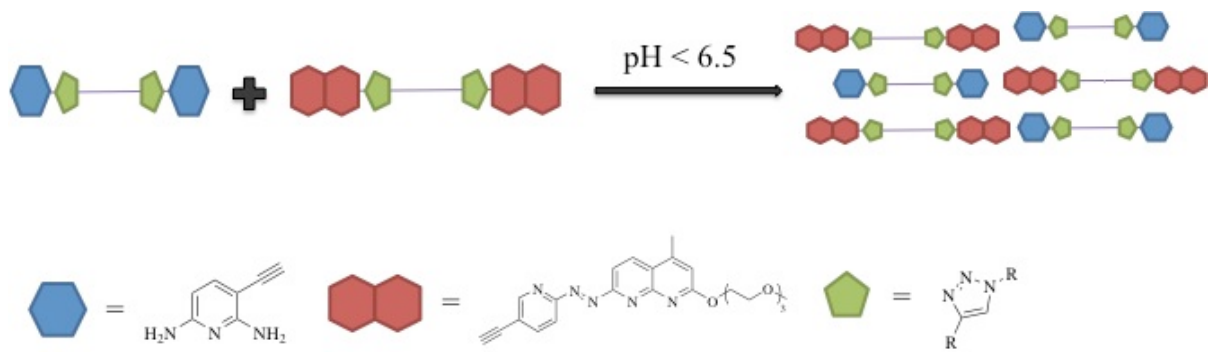
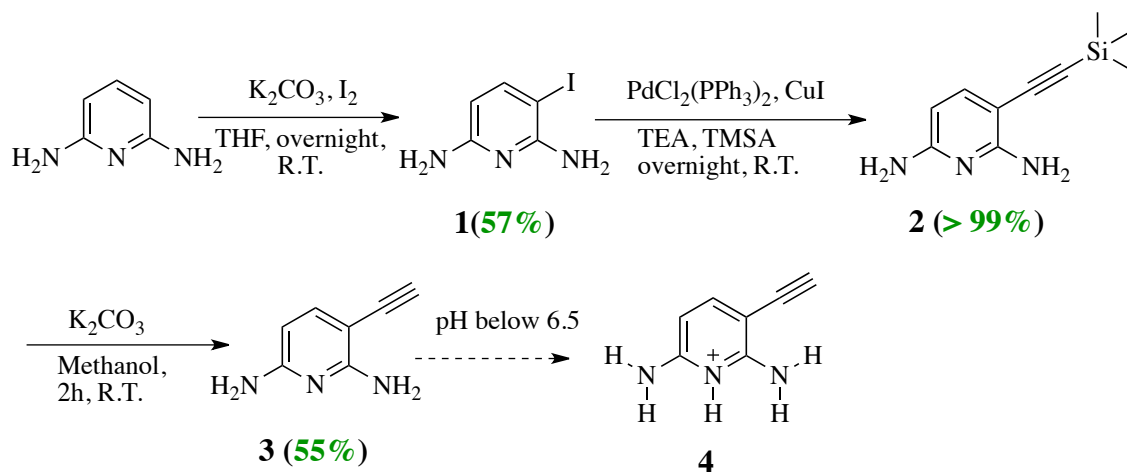


**Figure 12:** clicking donor and acceptor molecules to a bifunctional monomer.

## **Chapter 2: Results and Discussion**

## 2.1. Synthesis

### 2.1.1 Synthesis of Donor Molecule.

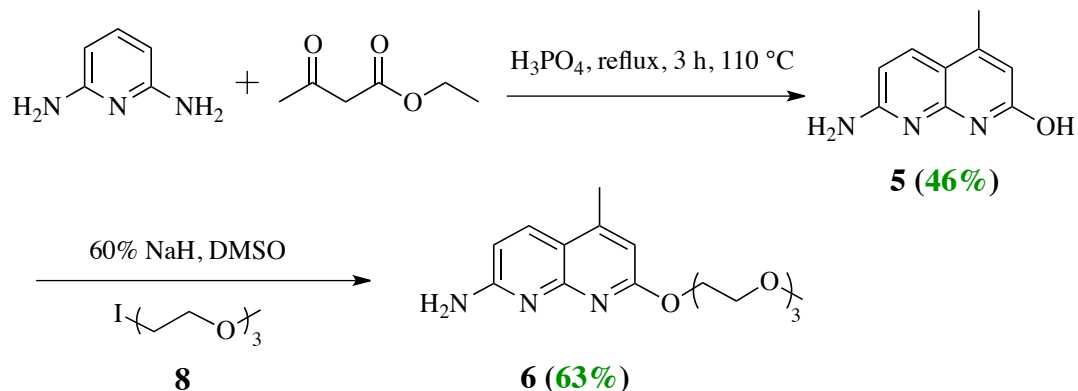


**Scheme 2:** Synthesis of the donor molecule.

2,6-diamino-3-ethynylpyridin-1-ium **4** was chosen as the DDD molecule and contains an alkyne functional group for eventual click chemistry to a covalent scaffold. The synthesis of **4** began with the iodination of commercially available, 2,6-diaminopyridine (Scheme 2). This reaction was performed based on a previously reported synthesis<sup>26</sup> and was monitored while adding iodine dropwise over 4 hours to avoid the formation of 3,5-diiodopyridine-2,6-diamine, since  $NH_2$  groups in positions 2 and 6 on the pyridine ring activate both carbons 3 and 5 for electrophilic aromatic substitution. A saturated aqueous solution of sodium thiosulfate was used in the workup to remove extra unreacted iodine, and the mixture was filtered through a celite pad to remove potassium iodide. A 57% yield of the monoiodo-pyridine-2,6-diamine was obtained and this yield was the best compared to other methods undertaken to obtain **1** and much easier. Sonogashira

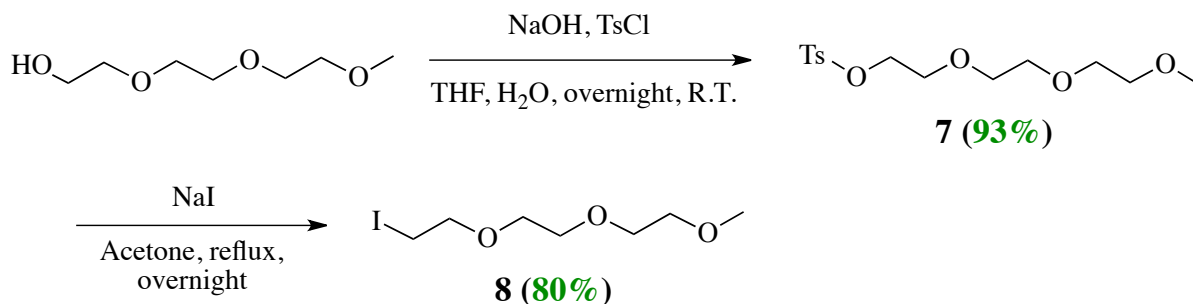
coupling was then used to convert **1** to **2** as a first step to attach the alkyne group.<sup>27</sup> The steps to produce **2** and **3** were performed very carefully using oven-dried glassware, deoxygenated solvents and a nitrogen atmosphere. Saturated aqueous sodium bicarbonate was used in the workup of the first step to neutralize the trace acid in the products and it gave a quantitative yield of **2**. Removal of the trimethylsilyl (TMS) protecting group was performed using 2 equivalents of  $K_2CO_3$  in methanol,<sup>28</sup> and gave a 55 % yield after recrystallization.

### 2.1.2 Synthesis of Acceptor molecule.



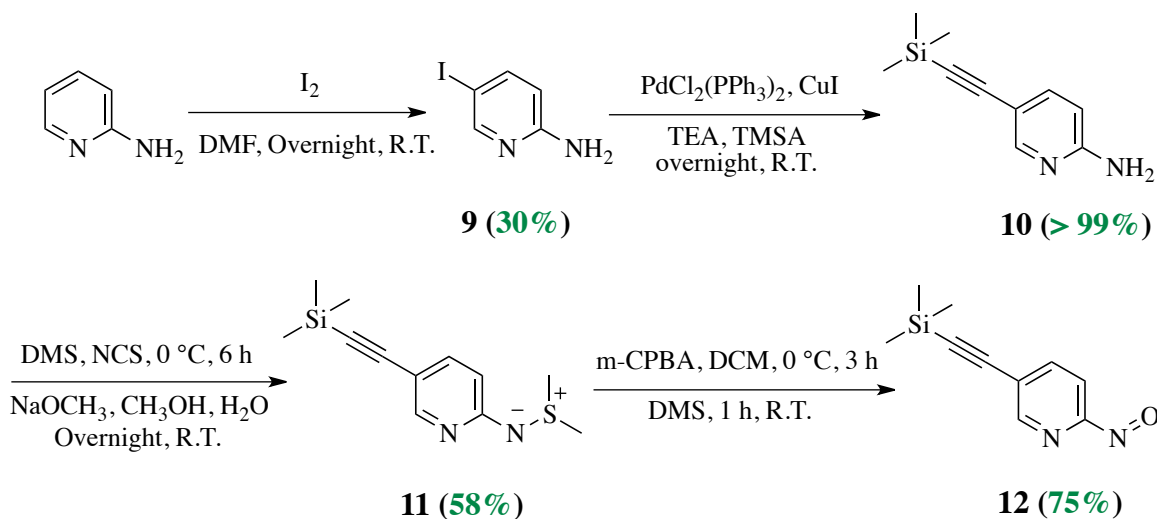
**Scheme 3:** Synthesis of **6**.

The synthesis of the acceptor subunit **14** began with the formation of **5** from a condensation between 2,6- diaminopyridine and ethyl acetoacetate in acidic conditions and a yield of 46% was obtained (Scheme 3).<sup>29,30</sup> Naphthyridine **5** work up was done by simple dilution and neutralization in water to precipitate the product in pure form most of the time. For further purification, recrystallization was performed on the recovered solid using acetone:diethyl ether (1:1). The nucleophilic substitution to form triethylene glycol derivative **6** was performed by adding 1-iodo-3,6,9-trioxodecane **8** within half an hour of adding base and the reaction was stirred overnight.



**Scheme 4: Synthesis of 8.**

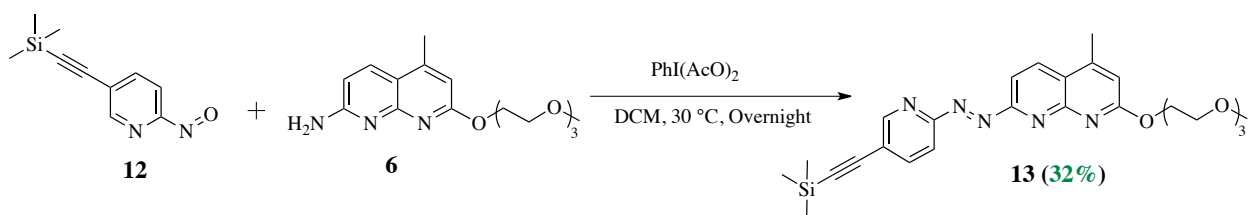
Iodo-3,6,9-trioxodecane **8** was synthesized to be a derivative of tri(ethylene glycol) bearing a good leaving group for the above described synthesis of **6** (Scheme 4). Both molecules **7** and **8** were prepared according to literature procedures.<sup>31,32</sup>



**Scheme 5: Synthesis of 12.**

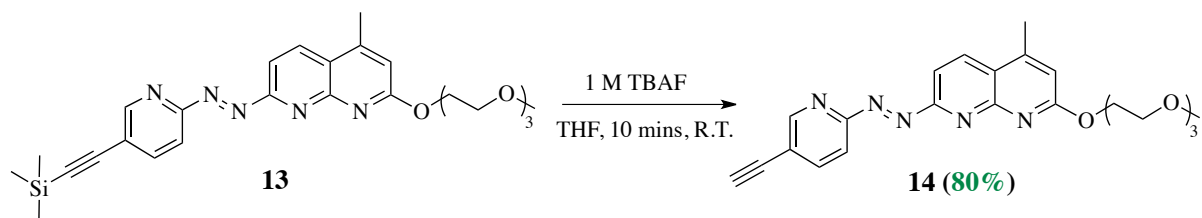
The synthesis of 5-iodo-2-nitrosopyridine, **9**, was initiated by iodination of 2-aminopyridine (Scheme 5). 2 equivalents of iodine were added all at once to 2-aminopyridine and the reaction was stirred overnight in DMF at room temperature.<sup>33</sup> A

saturated aqueous solution of sodium thiosulphate was added to remove the unreacted iodine and to neutralize the reaction mixture. This reaction was followed by a Sonogashira coupling reaction to afford **9** in a quantitative yield.<sup>34</sup> The sulfimine derivative **10** was synthesized by a previously reported method with a modification of the reaction time to obtain higher yield. Flash column chromatography was performed using EtOAc as eluent to yield 58% of **11**. Oxidation using 1.3 equivalent of *m*-chloroperbenzoic acid (*m*-CPBA) at 0 °C was performed to give **12** in 75% yield after addition of dimethylsulfide to remove the extra unreacted *m*-CPBA.<sup>35,36</sup> Workup of the reaction required evaporation at 20-30 °C to avoid producing a dimer. It has been shown in a previous study that 2-nitrosopyridine molecules exist in organic solvents as a mixture of the monomer and azodioxy dimer in equilibrium at room temperature.<sup>37</sup>



**Scheme 6:** Synthesis of **13**.

After the synthesis of **12** and **6**, the azo product (E)-2-(2-(2-(2-methoxyethoxy)ethoxy)ethoxy)-4-methyl-7-(((trimethylsilyl)ethynyl)pyridin-2-yl)diazanyl)-1,8-naphthyridine was synthesized from them using 1.3 equivalent of iodosobenzene diacetate (Scheme 6).<sup>38</sup> Purification by column chromatography using 4% methanol in DCM, eluent gave 32% of **13**.



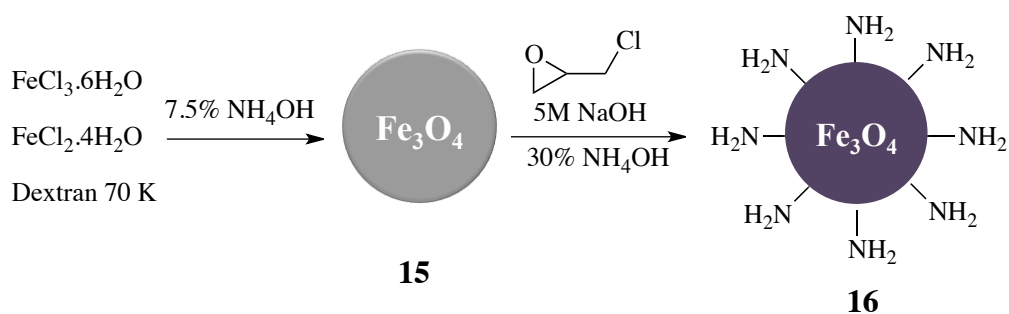
**Scheme 7:** Synthesis of the acceptor molecule, **14**.

Finally, 1 M tetra-*n*-butylammonium fluoride (TBAF) in THF was used to remove the trimethylsilyl (TMS) protecting group in **13** under dry conditions and in just 10 minutes, providing an 80% yield of the acceptor (Scheme 7).<sup>39</sup>



### 2.1.3 Synthesis of Dextran Coated Superparamagnetic Iron Oxide Nanoparticles

The synthesis of water soluble SPIO nanoparticles was performed using a previously reported method.<sup>40</sup> The first step involved the decomposition of  $\text{FeCl}_2$  and  $\text{FeCl}_3$  in the presence of ammonium hydroxide and dextran to produce water soluble dextran coated nanoparticles. As Weissleder and coworkers reported,<sup>6</sup> a cross-linked dextran shell with amine groups (Scheme 8) on the surface was synthesized, by using the previously synthesized coated nanoparticles and treating them first with epichlorohydrin and then aqueous ammonium hydroxide.



**Scheme 8:** Synthesis of dextran-coated  $\text{Fe}_3\text{O}_4$  nanoparticles.

Dynamic light scattering (DLS) was used to measure the sizes of the particles (Figure 13). The Z-average size was found to be 66 nm for the dextran-coated  $\text{Fe}_3\text{O}_4$  nanoparticles **15** and 77 nm for the cross-linked amine functionalized nanoparticles **16**.

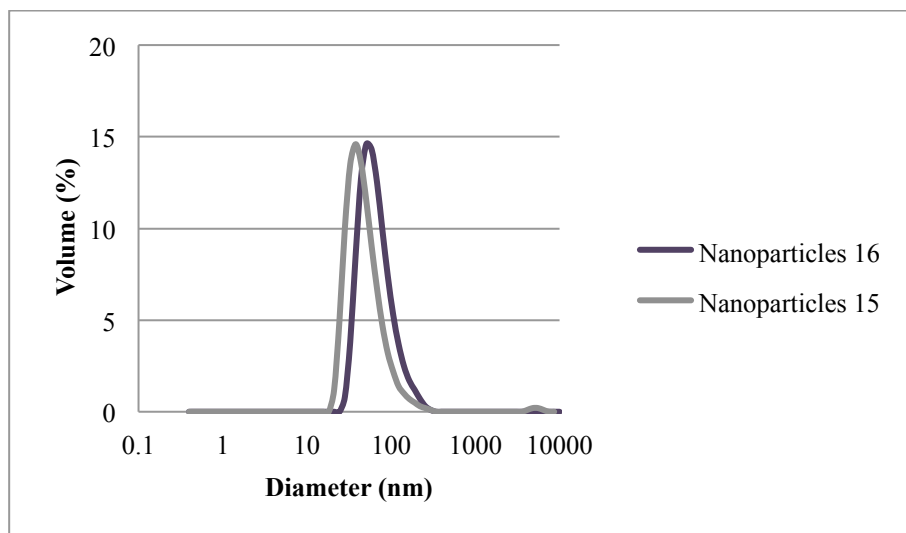


**Figure 13:** Size distribution of nanoparticles **15** (gray) and **16** (dark purple).

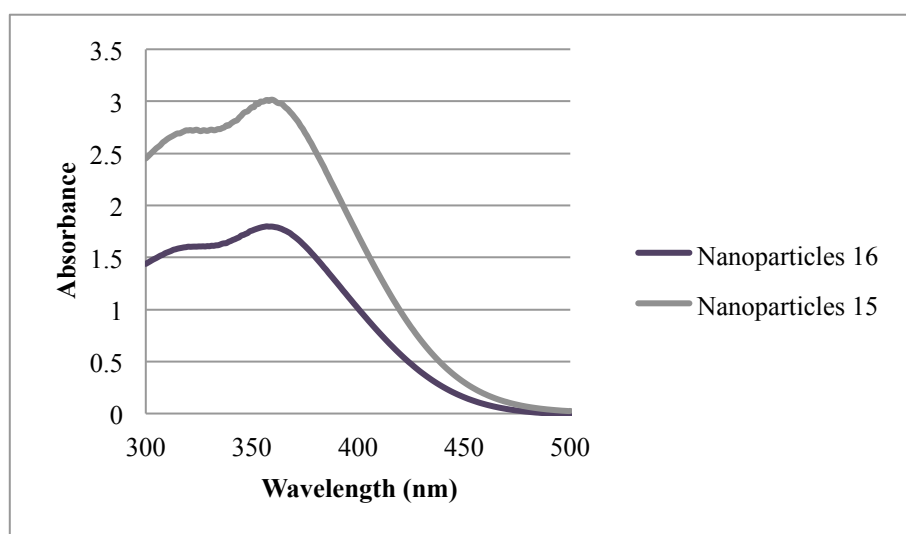
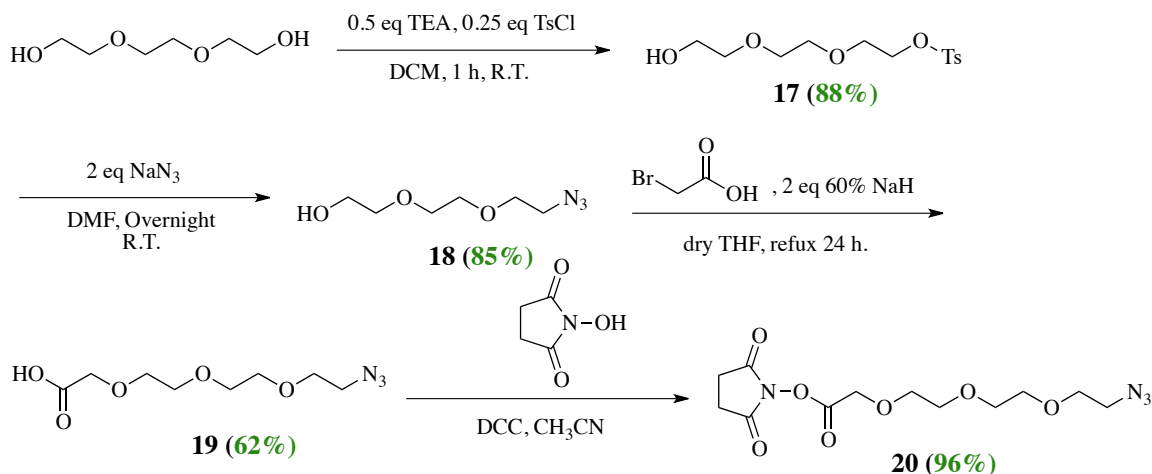


**Figure 24:** UV-Vis absorbance of nanoparticles **15** (gray) and **16** (dark purple).

UV-Vis absorption was also performed following nanoparticle degradation with hydrochloric acid and hydrogen peroxide on both nanoparticles **15** and **16** to determine the concentration of iron.<sup>41</sup> The calculation of concentration was based on the UV-Vis absorption that was found to be 3.01 at 365 nm for nanoparticles **15** corresponding to a concentration of 10.9 mg/mL and 1.80 at 365 nm for **16** corresponding to a concentration of 6.49 mg/mL.

#### 2.1.4 Synthesis of the linker.

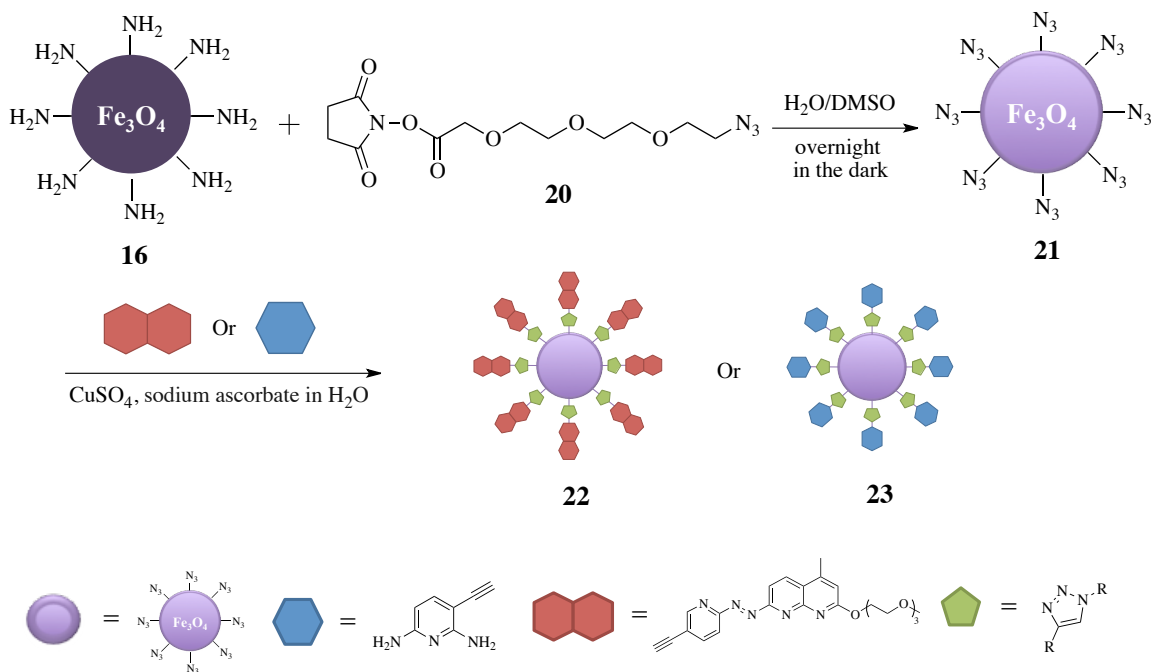


**Scheme 9:** Synthesis of the linker.

The synthesis of the linker for attachment of the hydrogen bonding moieties to the nanoparticles began with a monotosylation of tri(ethylene glycol) by reaction with 0.5 equivalents of triethylamine and 0.25 equivalents of 4-toluenesulfonyl chloride, affording 88% of **17** (Scheme 9).<sup>42</sup> Crude **17** was carried forward to the synthesis 2-(2-(2-azidoethoxy)ethoxy)ethanol, **18**, without any purification.<sup>43</sup> After reaction, flash column

chromatography was performed on the residue using 1:1 ethyl acetate:hexane as eluent, affording 85% of **18**. The carboxylic acid derivative **19** was synthesized by using sodium hydride (dispersion) as a base and alkylating the resulting oxo-anion with bromoacetate.<sup>44</sup> The final step to make the succinate ester linker, **20** was performed according to a literature procedure and afforded a similar yield.<sup>19</sup>

### 2.1.5 Conjugating donor and acceptor to nanoparticles



**Scheme 10:** Synthesis of the functionalized nanoparticles.

The next step in order to install the azide groups on the nanoparticles, was to react linker **20** with the cross-linked nanoparticles **16** (Scheme 10). This reaction was obtained by simply stirring 2.5  $\mu\text{mol}$  of linker **20** per milligram of iron at a pH of 7.4 overnight in the dark.<sup>19</sup> The pH was reached by performing a predialysis against 25 mM pH 7.4 citrate

buffer. The UV-visible absorbance was measured again following nanoparticle degradation with hydrochloric acid and hydrogen peroxide after performing dialysis of nanoparticles, **16** and for **21**. The absorption was found to be 1.34 at 365 nm corresponding to a concentration of 4.82 mg/mL for **16** and 0.508 at 365 nm corresponding to a concentration of 1.83 mg/ml for **21** (Figure 15). The Z-average size of particles **21** was found to be 90 nm (Figure 16). In addition, the presence of the azide groups on the nanoparticle surface was verified using infrared (IR) spectroscopy by the presence of the distinctive azide stretch at  $2100\text{ cm}^{-1}$  (Figure 17).

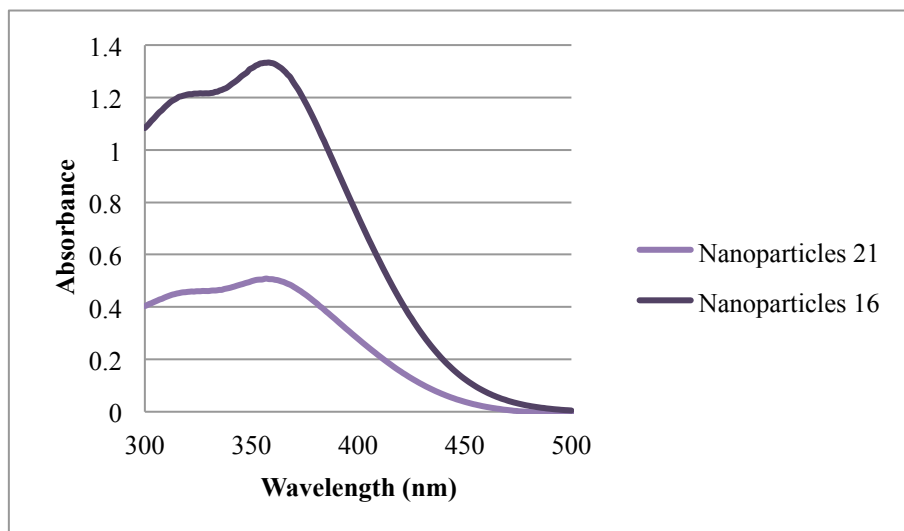


**Figure 15:** UV-Vis absorbance of nanoparticles **16** in pH 7.4 aqueous buffer (dark purple) and **21** (light purple).

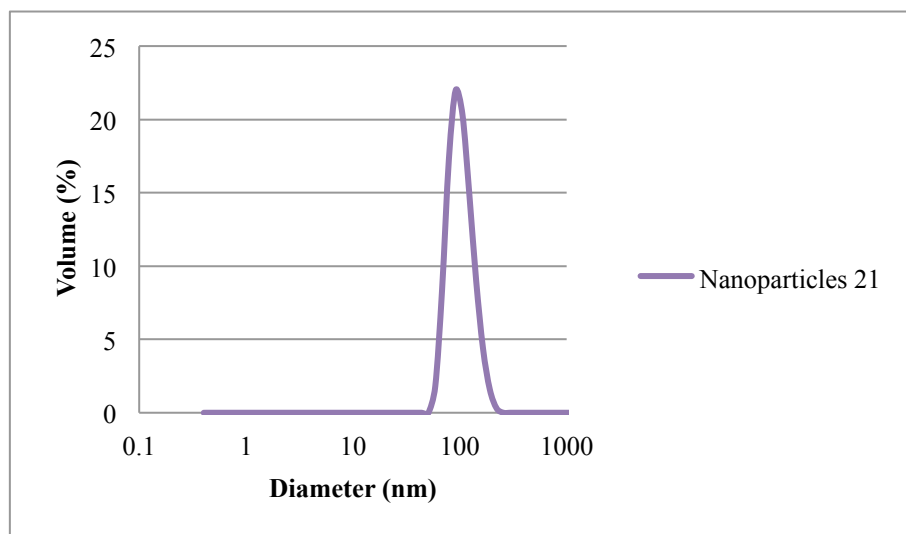


**Figure 16:** Size distribution of nanoparticles **21**.

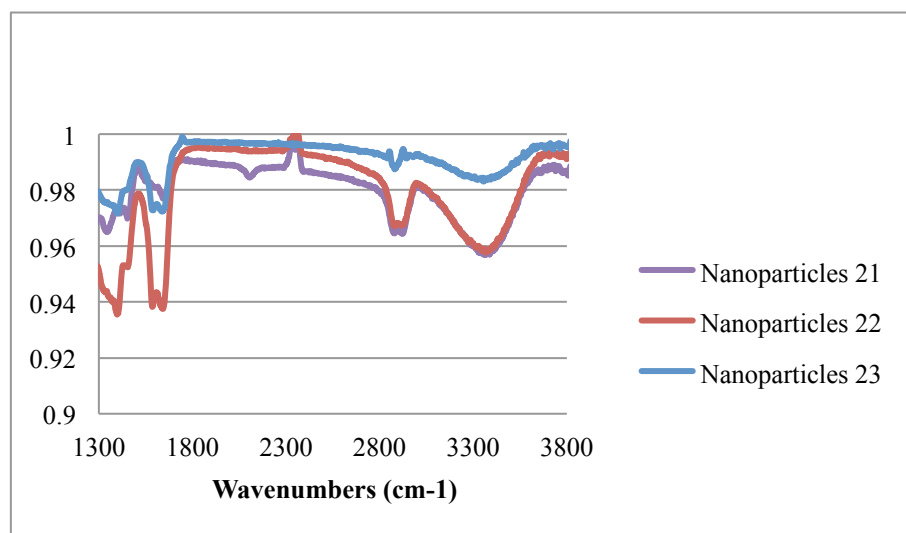


**Figure 17:** Infrared spectra illustrating changes on nanoparticle surface.

Finally, attachment of the donor and acceptor moieties to the surfaces of the nanoparticles was accomplished using a click reaction between their alkyne group and the

azide functions on the nanoparticles (Scheme 10). The click reaction was performed using  $\text{CuSO}_4$  and sodium ascorbate and dissolving the donor and acceptor molecules in DMF with the nanoparticles. The overnight reaction was followed by dialysis against 10 mM ethylenediaminetetraacetic acid (EDTA) to remove residual copper salts, followed by pure water.<sup>19</sup> The disappearance of the peak corresponding to the azide stretch was verified using infrared (IR) on the nanoparticles confirming completion of the reaction (Figure 17). The Z-average sizes of the particles were found to be 210 nm for **22** and 110 nm for **23** using DLS (Figure 18).

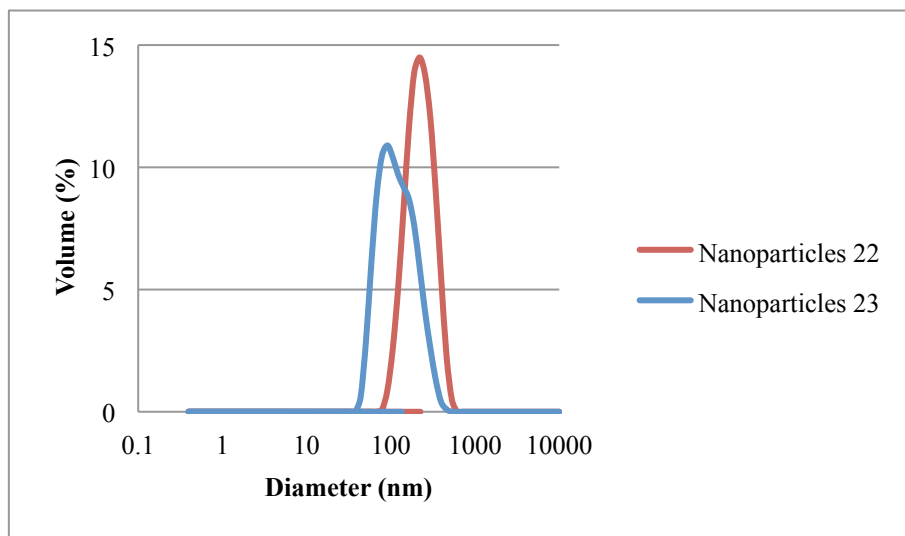
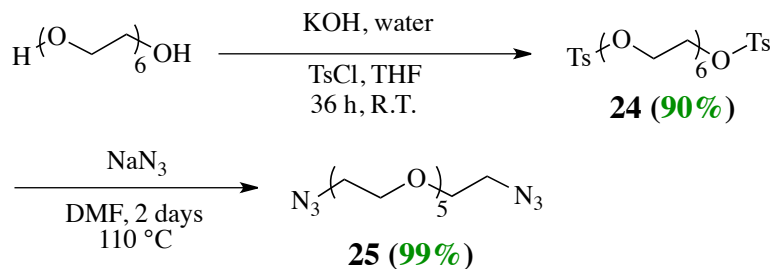


**Figure 18:** Size distribution of nanoparticles **22** (red) and **23** (blue).

18). 2.1.6 Synthesis of Donor and Acceptor monomers



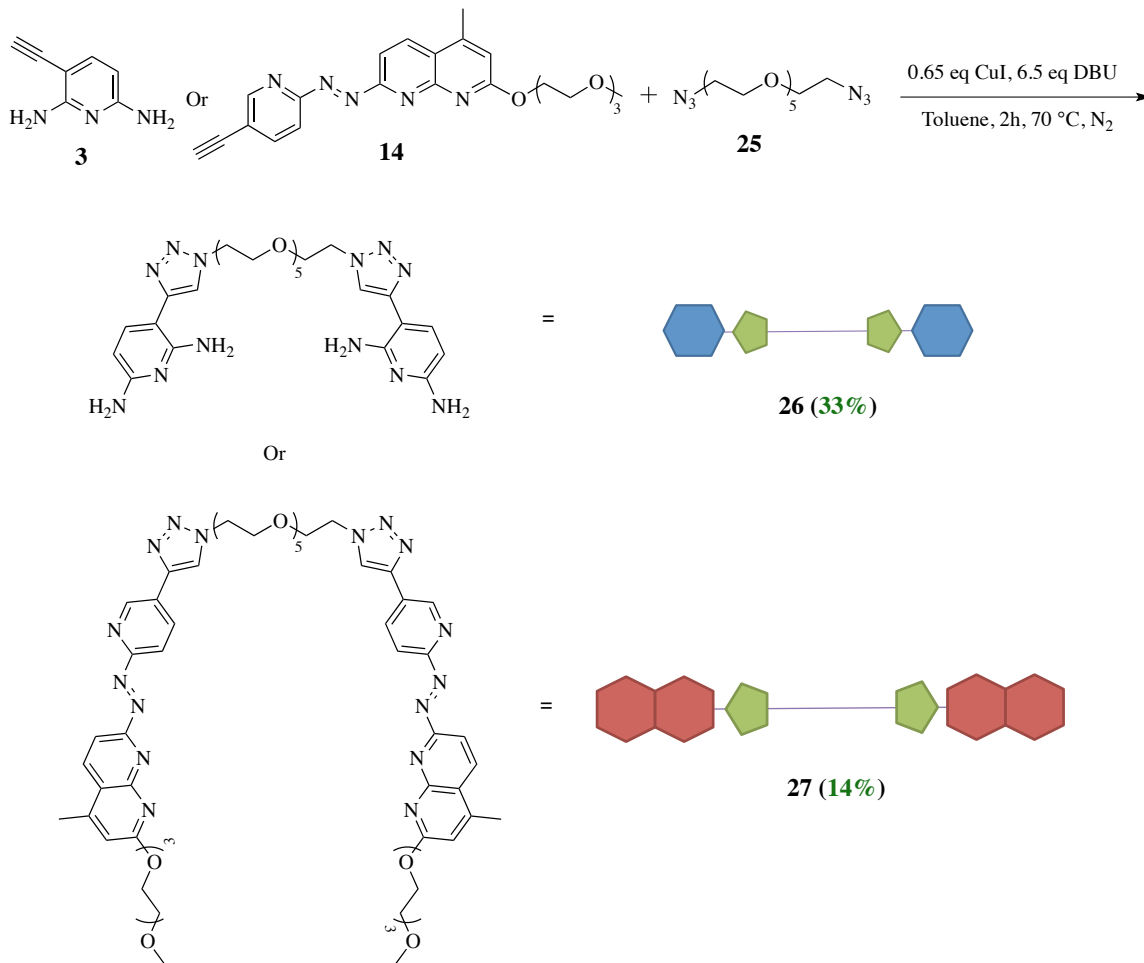
**Scheme 11:** Synthesis of the PEG derivative.

Synthesis of the PEG derivative **25** was necessary in order to do the click chemistry described above (Scheme 11). Synthesis of **24** was first performed by reacting hexa(ethylene glycol) with 6.6 equivalents of KOH and 2.5 equivalents of TsCl.<sup>45</sup> Recrystallization was performed to remove the mono tosylated derivatives. Compound **25** was synthesized according to a literature procedure.<sup>46</sup>

Donor and acceptor monomers were synthesized by click reactions (Scheme 12). The synthesis of the donor monomer **26** was performed by reaction between 2 equivalents of 3-ethynylpyridine-2,6-diamine **3** and 1 equivalent of **25**, while the acceptor monomer **27** was synthesized by reaction between 2 equivalents of (E)-7-((5-ethynylpyridin-2-yl)diazenyl)-2-(2-(2-(2-methoxyethoxy)ethoxy)ethoxy)-4-methyl-1,8-naphthyridine, **14** and 1 equivalent of **25**. Both click reactions were performed in the presence of 0.65 equivalents of CuI and 6.5 equivalents of 1,8-diazabicycloundec-7-ene (DBU).<sup>47</sup> Different workups were used for the two reactions due to the insolubility of the donor



monomer **26** in most organic solvents. A saturated solution of EDTA was required as a chelating agent to scavenge the metal ions in the workup.

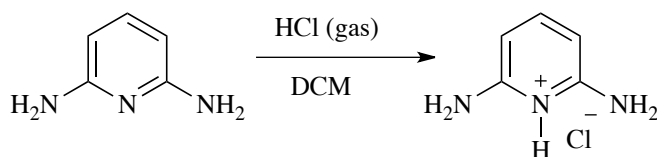


**Scheme 12:** Synthesis of the donor, **26** and Acceptor, **27** monomers.

## 2.2. pK<sub>a</sub> Titrations

### 2.2.1. pK<sub>a</sub> of the Donor Molecule.

Before starting the synthesis of **3**, a weak acid-strong base titration was performed to determine the pK<sub>a</sub> value for the nitrogen atom in the 2,6-diaminopyridine ring. This titration was performed by adding 1 mL of 0.1 M NaOH to 0.1 M of 2,6-diaminopyridin-1-ium chloride per minute and measuring the pH using a glass pH electrode at each time point. 2,6-Diaminopyridin-1-ium chloride was synthesized by the protonation of 2,6-diaminopyridine with HCl (gas) that was produced by adding H<sub>2</sub>SO<sub>4</sub> dropwise to NaCl (Scheme 13). Figure 19 shows the change in the pH while adding NaOH to 2,6-diaminopyridin-1-ium chloride and from the figure, the pK<sub>a</sub> can be determined which is likely very similar to the pK<sub>a</sub> for **3**.



**Scheme 13:** synthesizing 2,6-diaminopyridin-1-ium chloride.

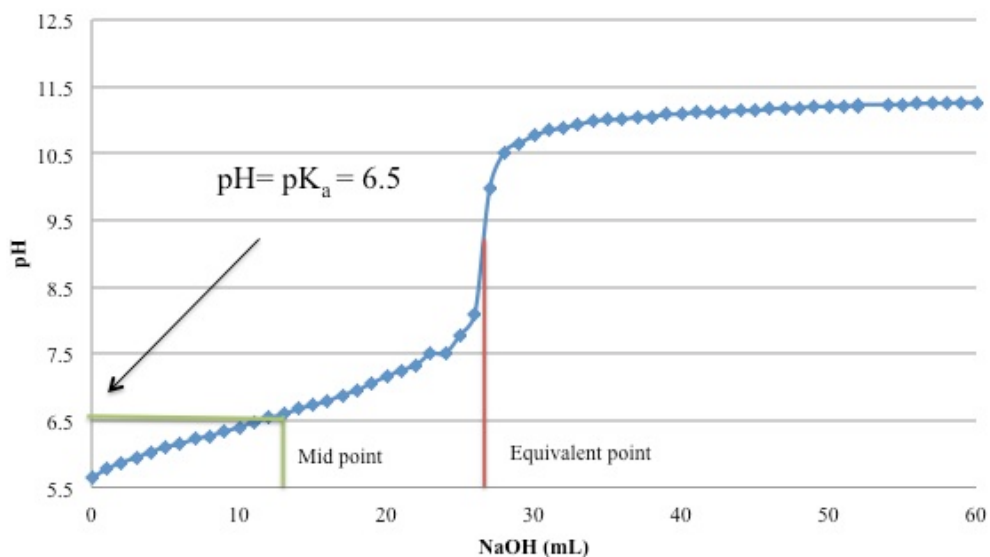


**Figure 19:** Weak acid-strong base titration of 2,6-diaminopyridinium chloride.

### 2.2.2. $pK_a$ of the Donor Monomer.

A weak acid-strong base titration was performed on **26** to determine the effect of the triazole group on the  $pK_a$  of the donor. This titration was performed by adding 1 mL of  $5 \times 10^{-4}$  M NaOH to  $5 \times 10^{-4}$  M of HCl salt of **26** per minute and measuring the pH using a glass pH electrode at each time point. The HCl salt of **26** was synthesized by dissolving **26** (0.1 g) in 0.1 M HCl (2 mL) and adding it dropwise to a saturated solution of NaCl (3 mL). Figure **20** demonstrates that the effect of adding a triazole group to the donor molecule changes the  $pK_a$  of the donor from 6.5 to 6.

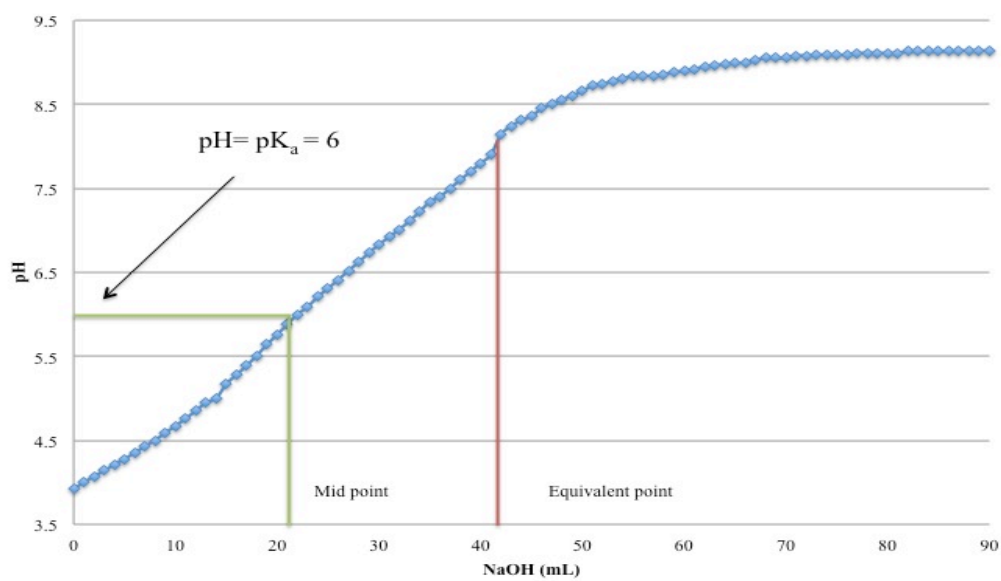


**Figure 20:** Weak acid-strong base titration of **26** HCl salt.

### 2.3. The Effect of Changing pH on the Aggregation of the Nanoparticles

The effect of changing pH on the aggregation of the nanoparticles was studied by measuring the Z-average size of 0.2 mg/mL nanoparticle solution (0.1 mg/mL of **22** + 0.1 mg/mL of **23**) at different pHs. The solution's pH was altered by adding  $1 \times 10^{-3}$  M HCl and  $1 \times 10^{-3}$  M NaOH and the pH was measured with a pH meter. This test was also performed on both nanoparticles **22** and **23** alone at the same iron concentration.

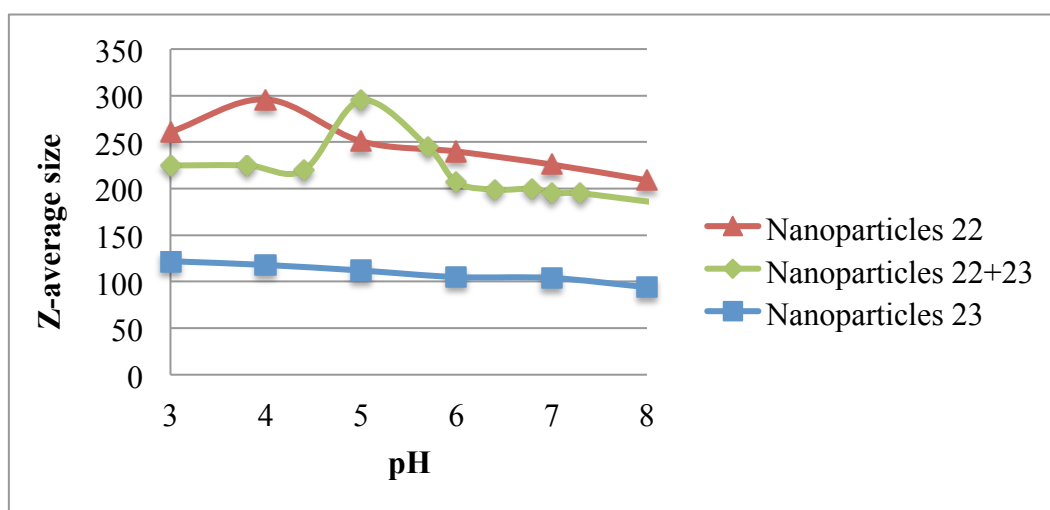


**Figure 21:** Z-average size changing with pH.

Figure **21** shows that an increase in the Z-average size of the nanoparticle mixture started at pH = 6 which is the  $pK_a$  of the donor molecule and reached the maximum size at 5.

The decrease in the size after that point may be due the start of protonation of the naphthyridine rings in the acceptor molecule. This protonation of the acceptor is responsible for the Z-average size increase between  $4 > \text{pH} > 3$  in nanoparticle **22**.

Although having these changes, they were not significant as we expected.

## 2.4. X-ray crystallography

An X-ray crystal structure was obtained for the acceptor **14** that explained the unexpected results of the aggregation tests (Figure 22).

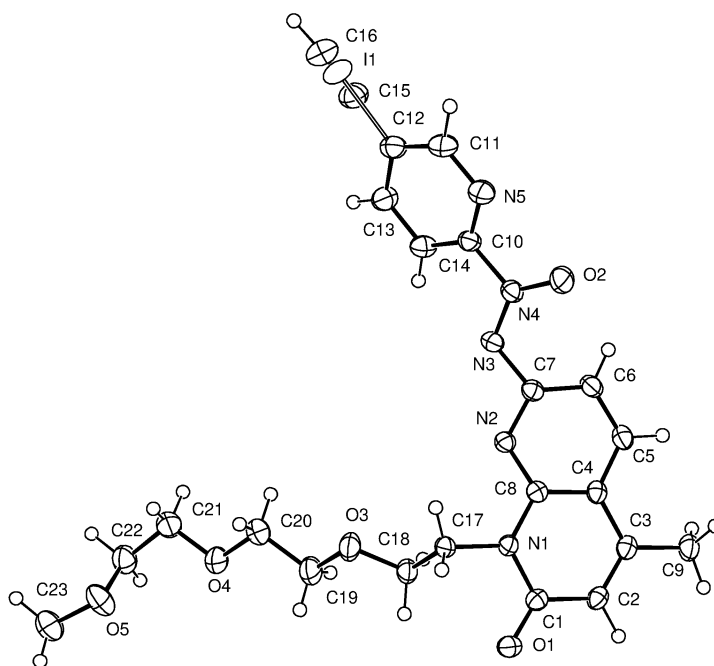
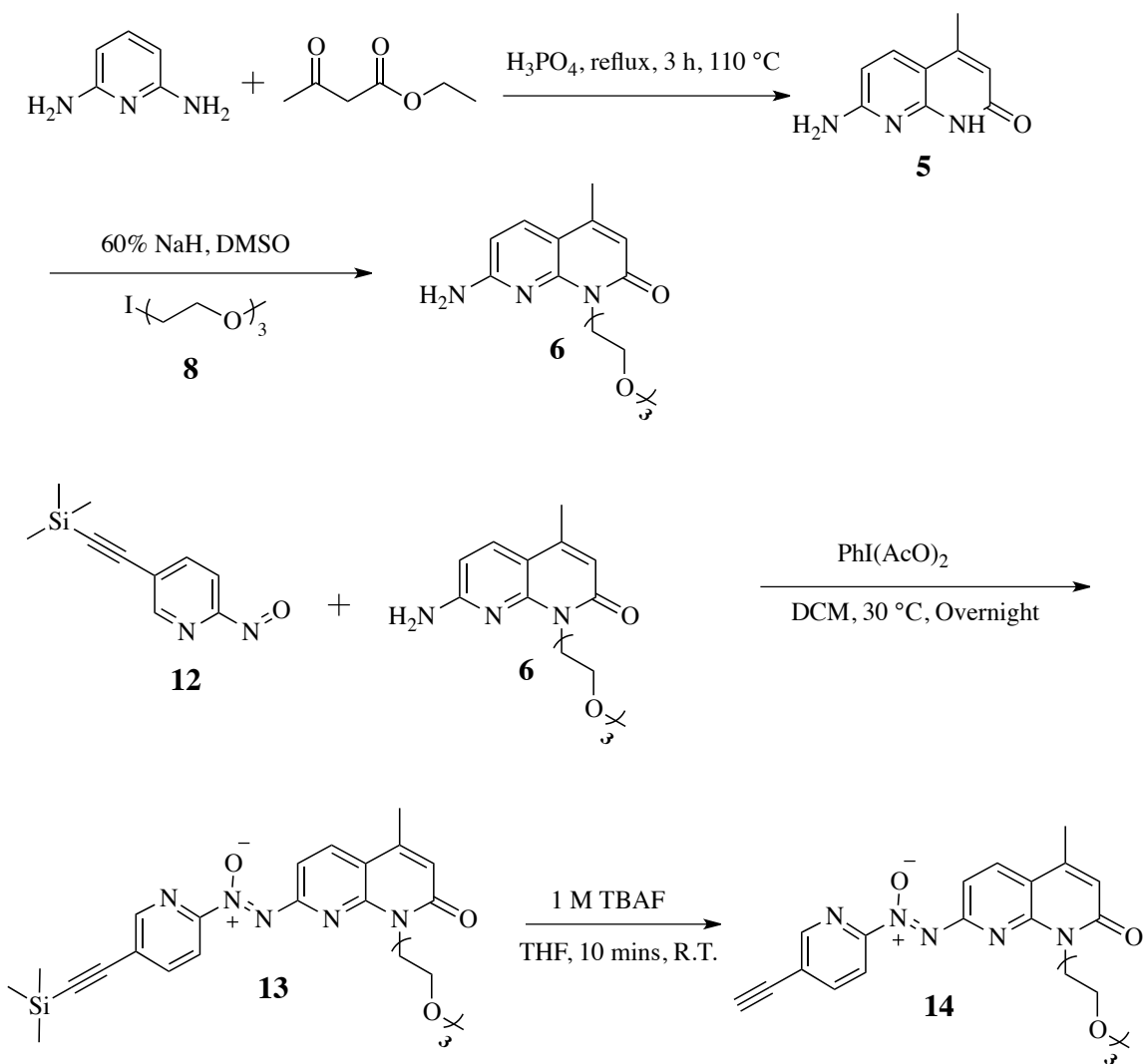


**Figure 22:** X-ray crystal structure of **14**.

Iodosobenzene diacetate was used to join the pyridine and naphthyridine components together but it was unclear whether an azo or azoxy bonds was created. MS was performed on the sample and showed an azo bond but it was not until this crystal structure was obtained that it was revealed that actually an azoxy bond was synthesized (N3=N4-O2). This structure also shows that TEG group was added at the nitrogen (N1)

instead of the oxygen (O1), a structural difference that was very difficult to elucidate by simple NMR spectroscopy. This improper placement blocks a hydrogen bonding site and disrupts the intended complexation with the donor. Based on the X-ray crystal structure of the acceptor molecule, the following revised scheme explains what happened in each step.



**Scheme 14:** synthesis of the acceptor

## 2.5. $^1\text{H}$ NMR Titration

An  $^1\text{H}$  NMR titration was performed between 2,6-diaminopyridinium tetrafluoroborate (donor) and (*E*)-2,4-dimethyl-7-(pyridin-2-ylidiazenyl)-1,8-naphthyridine (PAN) (acceptor). This complex (figure 23) is structurally similar to the desired system so the association constant will provide insight into the strength of the proposed complex. It was performed in DMSO, which is a very competitive solvent, and we obtained a  $K_a$  value of  $194\text{ M}^{-1}$ .

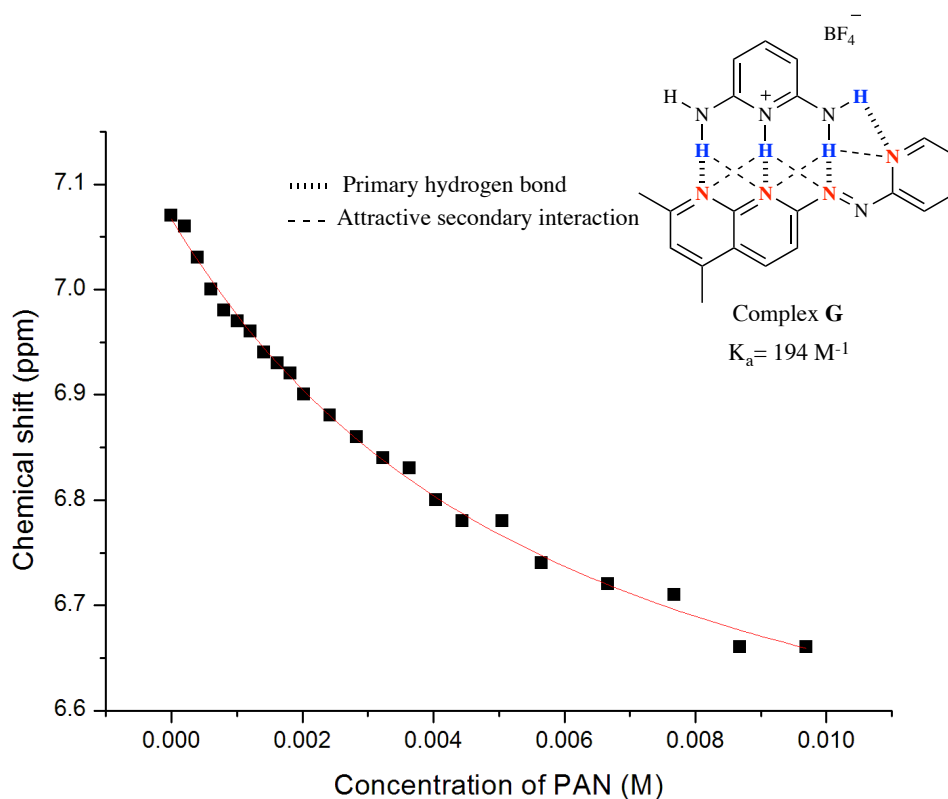


**Figure 23:** Titration curve for complex G.



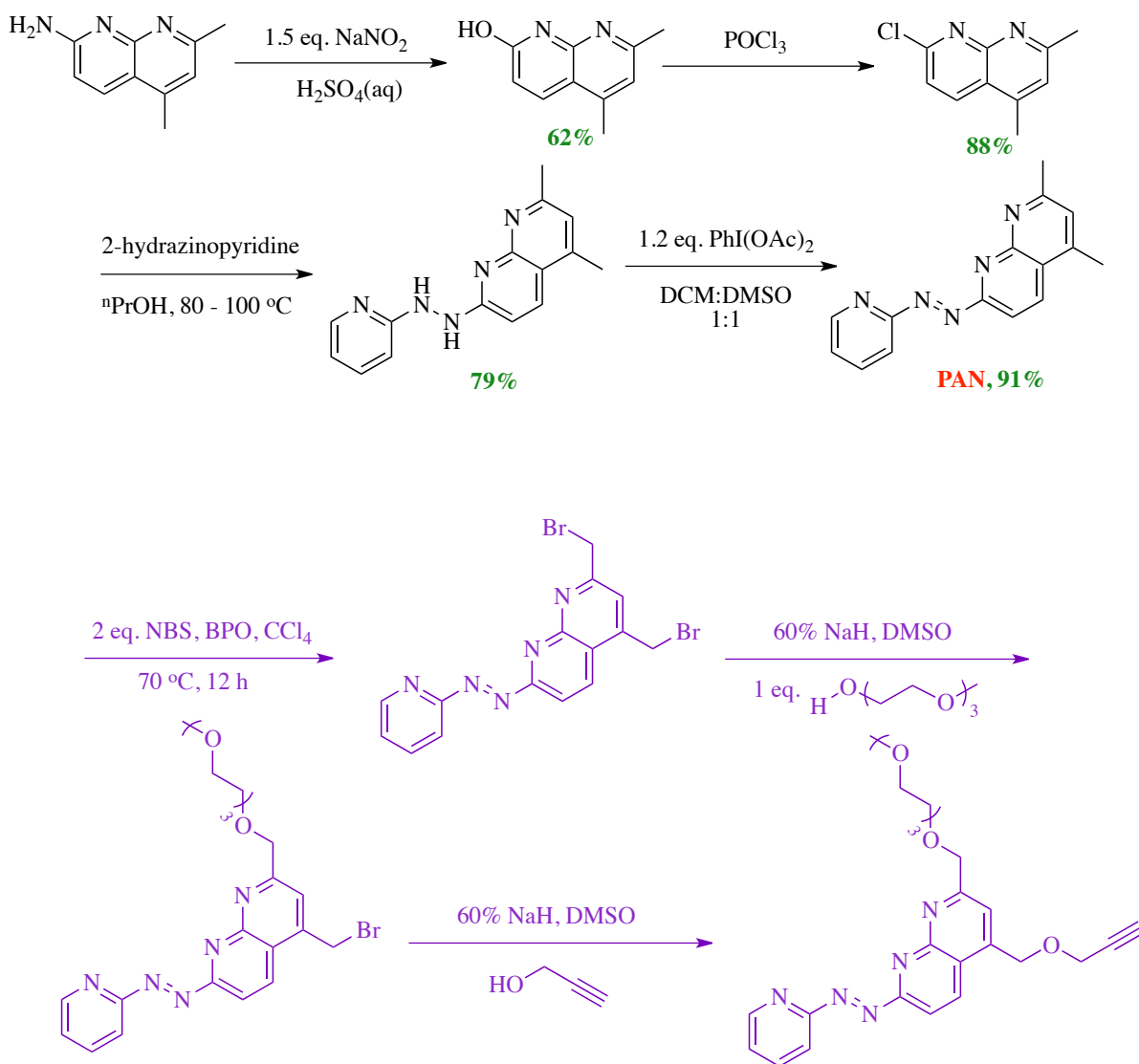
## **Chapter 3: Conclusions and Future Work**

This thesis explored the synthesis of donor and acceptor hydrogen bonding moieties for conjugation to SPIO. The aim was to develop a system that would undergo aggregation in the mildly acidic environment of tumors, in order to provide enhanced contrast. Though there were a few previous examples of controlled clustering of such nanoparticles in the presence of stimuli, clustering induced by very small pH changes had not previously been demonstrated. The donor molecule was successfully synthesized in three simple steps including a Sonogashira coupling and deprotection of the TMS group. The acceptor molecule synthesis involved the preparation of an amine derivative and a nitroso derivative. Then, both derivatives were oxidized to obtain the azo group and followed by deprotection of the TMS group. SPIO were synthesized and then cross-linked after coating them with dextran. A linker was synthesized to obtain azide group on the surface of the SPIO for further click reaction with the donor and acceptor molecules.

Donor and acceptor molecules were added to azide functionalized SPIO via click chemistry. After conjugation to the nanoparticle surface, the results of clustering mixed nanoparticles within the accessible tumor pH range were not significant. The presence of the TEG group on one nitrogen atom in the naphthyridine ring and oxygen on the azo group unexpectedly was revealed by x-ray crystallography during the final stages of this thesis. This made the acceptor molecule too weak to form a strong complex, explaining the lack of SPIO clustering. However, the idea of this project may be worth carrying forward based on the strength of a similar complex that showed good binding strength in DMSO.

Although synthesizing non-symmetrical azo heterocyclic molecules has proven to be difficult, the Wisner group has recently developed a method to do so. Scheme 15

shows a successful route without achieving an azoxy as an intermediate and adopting this procedure is highly recommended for completion of this project. The PAN molecule (Scheme 15) was successfully synthesized by a Ph.D. candidate Jeffrey Pleizier in the Wisner group and the rest of the scheme is a suggested synthesis for an alternative acceptor molecule.<sup>48,49,50,51</sup>



**Scheme 15:** Suggested future work.

## **Chapter 4: Experimental**

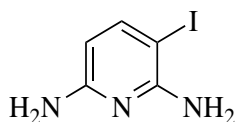
#### 4.1. General:

All chemicals were of reagent quality and used as obtained from commercial sources unless otherwise noted. Dry solvents were obtained from an Innovative Technology SPS-400-5 Solvent Purification System. Flasks were oven dried and nitrogen-purged prior to use. Reactions were carried out under an inert atmosphere (dry nitrogen) unless otherwise indicated. Flash chromatography was performed using Silicycle pharma grade silica (40-63 $\mu$ m). Dialysis was performed against water using a Spectra/Por regenerated cellulose membrane (12-14,000 MW cutoff). Ultrafiltration was carried out using a 300 KDa molecular weight cutoff (MWCO) membrane of regenerated cellulose purchased from Amicon. The  $^1\text{H}$  and  $^{13}\text{C}$  NMR data were obtained on 400 or 600 MHz spectrometers. All spectra were obtained in deuterated chloroform and/or DMSO- $d_6$ . The spectra were referenced to residual chloroform (at  $\delta$  7.25 ppm for  $^1\text{H}$  spectra and the center peak of the triplet at  $\delta$  77.0 (t) for  $^{13}\text{C}$  spectra) and DMSO- $d_6$  (at  $\delta$  2.49 ppm for  $^1\text{H}$  spectra and the center peak of the multiplet at  $\delta$  39.50 (m) for  $^{13}\text{C}$  spectra). When peak multiplicities are given, the following abbreviations are used: s, singlet; d, doublet; t, triplet; q, quartet; m, multiplet; EI (electron ionization) mass spectra were obtained on Finnigan MAT 8200 and PE-Sciex API 365 mass spectrometers at an ionizing voltage of 70 eV.

## 4.2 Experimental Section

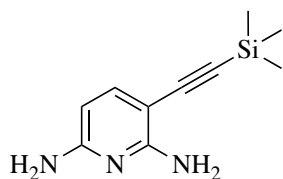
### 4.2.1 Synthesis of Donor Molecule

#### 3-Iodo-pyridine-2,6-diamine (1).



A suspension of 2,6-diaminopyridine (10.01 g, 0.091 mol) and potassium carbonate (12.65 g, 0.091 mol) in THF (100 mL) was stirred for 1 hour. A solution of iodine (23.3 g, 0.091 mol) in THF (50 mL) was added dropwise over 4 hours to the suspension. The reaction mixture was stirred overnight at room temperature. After the reaction time, the resulting residue was filtered through a celite pad and the filtrate was washed with water and a saturated aqueous solution of sodium thiosulphate to remove the extra-unreacted iodine. The organic layer was dried over potassium carbonate and evaporated under reduced pressure affording a gray solid of the title compound **1** (12.24 g, 57 %). <sup>1</sup>H NMR (CDCl<sub>3</sub>, 400 MHz): δ 4.22 (s, 2H), 4.68 (s, 2H), 5.72 (d, 1H, *J*=8.2), 7.50 (d, 1H, *J*=8.2). <sup>13</sup>C NMR (400 MHz, CDCl<sub>3</sub>): δ 61, 100.5, 147.9, 156.3, 157.6. HRMS calcd for C<sub>5</sub>H<sub>6</sub>IN<sub>3</sub> [M]<sup>+</sup>: 234.9606, found: 234.9607.

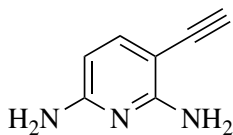
#### 3-(Trimethylsilyl)ethynyl pyridine-2,6-diamine (2).



3-Iodo-pyridine-2,6-diamine (**1**, 12.0 g, 51.0 mmol), PdCl<sub>2</sub>(PPh<sub>3</sub>)<sub>2</sub> (0.35 g, 0.51 mmol, 1.0 mol %), and CuI (0.19 g, 0.99 mmol, 2.0 mol %) were charged in an oven-dried, nitrogen-purged 250 mL round bottom flask under N<sub>2</sub> atmosphere. Triethylamine (100 mL) which was deoxygenated by being bubbled with N<sub>2</sub> gas for 30 minutes was added via syringe followed by the addition of TMSA (5.99 g, 61.01 mmol). The reaction stirred overnight

under N<sub>2</sub> at room temperature. After reaction time, solvent was removed under reduced pressure. Saturated aqueous sodium bicarbonate (50 mL) was added to the residue and chloroform (100 mL). The mixture was further extracted with chloroform (3 x 20 mL). The combined organic layers were dried over potassium carbonate and evaporated under reduced pressure to obtain dark brown solid of the titled compound **2** (10.4 g, 100%). <sup>1</sup>H NMR (CDCl<sub>3</sub>, 400 MHz): δ 0.23 (s, 9H), 4.36 (s, 2H), 4.82 (s, 2H), 5.81 (d, 1H, *J*=8.2), 7.31 (d, 1H, *J*=8.2). <sup>13</sup>C NMR (400 MHz, CDCl<sub>3</sub>): δ 0.13, 97.7, 98, 101.7 141.9, 157.4, 159.2. HRMS calcd for C<sub>10</sub>H<sub>15</sub>N<sub>3</sub>Si [M]<sup>+</sup>: 205.1035, found: 205.1037.

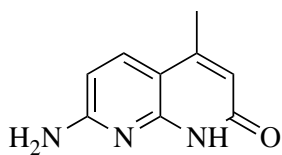
3-Ethynylpyridine-2,6-diamine (3).



To 3-(trimethylsilyl ethynyl) pyridine-2,6-diamine (**2**, 10.4 g, 50.65 mmol) and potassium carbonate (13.99 g, 101.3 mmol), methanol (100 mL) which was deoxygenated by being bubbled with N<sub>2</sub> gas for 30 minutes was added under N<sub>2</sub>. The reaction solution stirred for 2 hours at room temperature. After reaction, the solution was evaporated under reduced pressure and the remaining residue was dissolved in chloroform and diluted with water. Extraction was performed with chloroform (3 x 50 mL). The combined organic layers were dried over potassium carbonate and evaporated under reduced pressure to afford (3.6 g, 55%) of the donor molecule after recrystallization using chloroform: hexane. <sup>1</sup>H NMR (CDCl<sub>3</sub>, 400 MHz): δ 3.31 (s, 1H), 4.36 (s, 2H), 4.81 (s, 2H), 5.84 (d, 1H, *J*=8.2), 7.34 (d, 1H, *J*=8.2). <sup>13</sup>C NMR (400 MHz, CDCl<sub>3</sub>): δ 80.5, 81.1, 97.8, 142.3, 157.6, 159.5. HRMS calcd for [M]<sup>+</sup> calc'd for C<sub>7</sub>H<sub>7</sub>N<sub>3</sub>: 133.0640, found: 133.0643

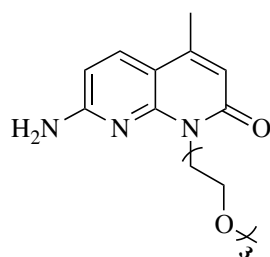
## 4.2.2 Synthesis of Acceptor Molecule.

### 7-Amino-2-hydroxy-4-methyl-1,8-naphthyridine (5).



2,6-Diaminopyridine (32.74 g, 300.01 mol) and ethyl acetoacetate (39.05 g, 300.01 mol) were heated in phosphoric acid (130 mL) for 3 hour at 110 °C. After cooling to room temperature, the solution was poured into distilled water and neutralized by adding ammonium hydroxide until pH: 7 and filtered affording a beige solid (24.03 g, 45.6 %) of the titled product **5**.  $^1\text{H}$  NMR (DMSO, 400 MHz):  $\delta$  2.27 (s, 3H), 5.99 (s, 1H), 6.33 (d, 1H,  $J=8.6$ ), 6.66 (s, 2H), 7.69 (d, 1H,  $J=8.6$ ). HRMS calcd for  $\text{C}_9\text{H}_9\text{N}_3\text{O}$   $[\text{M}]^+$ : 175.0746, found: 175.0748.

### Functionalized Naphthyridine (6).

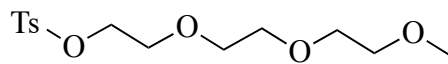


To 7-amino-2-hydroxy-4-methyl-1,8-naphthyridine (**5**, 1.02 g, 5.8 mmol) in DMSO (50 mL), 60 % sodium hydride (0.23 g, 5.8 mmol) was added to the solution carefully under  $\text{N}_2$ . After 30 minutes, 1-iodo-3,6,9-trioxodecane (**8**, 1.58 g, 5.8 mmol) was added via syringe and reaction stirred overnight under  $\text{N}_2$  at room temperature. After reaction time, the solution was poured into distilled water and extracted many times with dichloromethane. The organic layers were combined and washed with distilled water and dried over potassium carbonate. The solvent was removed by rotary evaporation affording a brown oil (1.17 g, 62.9 %) of the titled product **6**.  $^1\text{H}$  NMR ( $\text{CDCl}_3$ , 400 MHz):  $\delta$  2.31 (s, 3H), 3.36 (s, 3H), 3.51-3.53 (m, 2H), 3.60-3.63 (m, 4H), 3.70-3.72 (m, 2H), 3.75 (t, 2H,  $J=6.6$ ), 4.63 (t, 2H,  $J=6.6$ ) 4.97 (s, 2H), 6.29 (s, 1H), 6.36 (d, 1H,

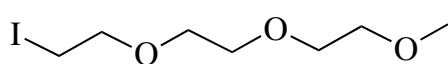


$J=8.6$ ), 7.66 (d, 1H,  $J=8.6$ ).  $^{13}\text{C}$  NMR (400 MHz,  $\text{CDCl}_3$ ):  $\delta$  17.9, 39, 58.5, 67.4, 69.7, 69.9, 71.4, 103.9, 107.4, 115.1, 134.3, 145.7, 149, 158.6, 162.8. HRMS calcd for  $\text{C}_{16}\text{H}_{23}\text{N}_3\text{O}_4$   $[\text{M}]^+$ : 321.1689, found: 321.1685.

1-(p-Tolylsulfonyl)-3,6,9-trioxodecane (7).

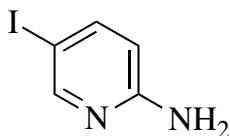
 To sodium hydroxide (5.72 g, 80.0 mmol) in water (20 mL), tri(ethylene glycol) monomethyl ether (13.26 g, 80.0 mmol) in dry THF (20 mL) was added under  $\text{N}_2$ . The flask was cooled in an ice bath with stirring and a solution of 4-toluenesulfonyl chloride (15.28 g, 80.0 mmol) in THF (24 mL) was added dropwise over 30 minutes. After addition, the reaction stirred under  $\text{N}_2$  at room temperature overnight. After the reaction time, distilled water was added to the residue and was neutralized using sulfuric acid and solution was extracted many times with DCM. The combined organic layers were washed with distilled water and dried over potassium carbonate. The organic layer was evaporated under reduced pressure affording a clear colorless oil of the title product **7** (23.67 g, 92.9 %).  $^1\text{H}$  NMR ( $\text{CDCl}_3$ , 400 MHz):  $\delta$  2.21 (s, 3H), 3.12 (s, 3H), 3.27-3.29 (m, 2H), 3.34 (s, 4H), 3.35-3.38 (m, 2H), 3.44 (t, 2H,  $J=4.3$ ), 3.93 (t, 2H,  $J=4.3$ ), 7.14 (d, 2H,  $J=8.2$ ), 7.56 (d, 2H,  $J=8.2$ );  $^{13}\text{C}$  NMR (400 MHz,  $\text{CDCl}_3$ ):  $\delta$  20.7, 58.0, 67.8, 68.7, 69.6, 69.8, 71, 127.1, 129.1, 132.2, 144.1. HRMS calcd for  $\text{C}_{14}\text{H}_{22}\text{O}_6\text{S}$   $[\text{M}]^+$ : 318.1137, found: 318.1132.

1-Iodo-3,6,9-trioxodecane (8).

 1-(p-Tolylsulfonyl)-3,6,9-trioxodecane, **7** (10.0 g, 31.4 mmol) and sodium iodide (9.9 g, 66.0 mmol) were dissolved in acetone (80 mL) and refluxed overnight under  $\text{N}_2$ . After reaction, the

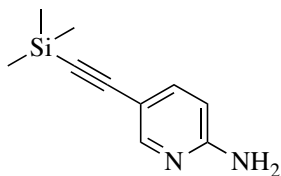
solution was filtered. After the evaporation of solvent, the residue was diluted with DCM. The organic layer was washed with aqueous sodium thiosulfate then brine (2 x each) and dried over sodium sulfate. The organic layer was removed by rotary evaporation affording a yellowish oil (6.9 g, 80.2 %) of the titled product **8**.  $^1\text{H}$  NMR ( $\text{CDCl}_3$ , 400 MHz):  $\delta$  2.99 (t, 2H,  $J=6.8$ ), 3.09 (s, 3H), 3.25-3.27 (m, 2H), 3.35-3.38 (m, 6H), 3.48 (t, 2H,  $J=6.8$ );  $^{13}\text{C}$  NMR (400 MHz,  $\text{CDCl}_3$ ):  $\delta$  2.7, 58.6, 69.8, 70.19, 70.2, 71.54, 71.55. HRMS calcd for  $\text{C}_7\text{H}_{15}\text{IO}_3$   $[\text{M}]^+$ : 274.0066, found: 274.0153

5-Iodo-2-aminopyridine (9).



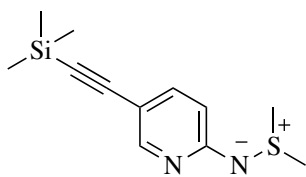
To 2-aminopyridine (20.0 g, 212.0 mmol) in DMF (200 mL), iodine (53.8 g, 424.0 mmol) was added and the mixture was stirred overnight at room temperature. The resulting mixture was poured into another mixture of 12 g sodium metabisulfate in 120 mL ammonium hydroxide and aqueous sodium thiosulfate. The product was extracted many times with DCM and the combined organic layers were dried using  $\text{MgSO}_4$  and evaporated under reduced pressure. The resulting residue was recrystallized using DCM: Hexane. The resulting golden solid was filtered and air dried to afford (14.0 g, 30 %) of the compound **9**.  $^1\text{H}$  NMR ( $\text{CDCl}_3$ , 400 MHz):  $\delta$  4.45 (s, 2H), 6.36 (d, 1H,  $J=8.6$ ), 7.63 (d, 1H,  $J=8.6$ ), 8.23 (s, 1H).  $^{13}\text{C}$  NMR (400 MHz,  $\text{CDCl}_3$ ):  $\delta$  77.7, 110.8, 145.2, 153.7, 157.2. HRMS calcd for  $\text{C}_5\text{H}_5\text{IN}_2$   $[\text{M}]^+$ : 219.9497, found: 219.9506.

5-((Trimethylsilyl)ethynyl)pyridin-2-amine (10).



5-Iodo-2-aminopyridine (**9**, 12.7 g, 57.8 mmol), PdCl<sub>2</sub>(PPh<sub>3</sub>)<sub>2</sub> (0.4 g, 0.57 mmol, 1.0 mol %), and CuI (0.22 g, 1.1 mmol, 2.0 mol %) were charged in an oven-dried, nitrogen-purged 250 mL round bottom flask under N<sub>2</sub> atmosphere. Triethylamine (150 mL) which was deoxygenated by being bubbled with N<sub>2</sub> gas for 30 minutes was added via syringe followed by the addition of TMSA (6.8 g, 69.2 mmol). The reaction was stirred at room temperature overnight under N<sub>2</sub>. After the reaction time, solvent was then removed under reduced pressure. Saturated aqueous sodium bicarbonate (50 mL) was added to the residue and chloroform (100 mL). The mixture was further extracted with chloroform (3 x 50 mL). The combined organic layers were dried over potassium carbonate and evaporated under reduced pressure to obtain a brownish solid (10.9 g, 100%) of the title product **10**. <sup>1</sup>H NMR (CDCl<sub>3</sub>, 400 MHz): δ 0.21 (s, 9H), 4.77 (s, 2H), 6.41 (d, 1H, *J*=8.6), 7.46 (d, 1H, *J*=8.6), 8.18 (d, 1H). <sup>13</sup>C NMR (400 MHz, CDCl<sub>3</sub>): δ 0, 94.4, 102.7, 107.7, 109.6, 140.6, 151.8, 157.5. HRMS calcd for C<sub>10</sub>H<sub>14</sub>N<sub>2</sub>Si [M]<sup>+</sup>: 190.0926, found: 190.0930.

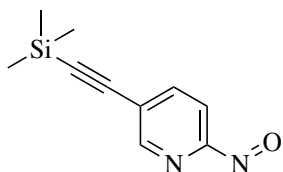
5-((Trimethylsilyl)ethynyl)pyridin-2-sulfimine (11).



To 5-((trimethylsilyl)ethynyl)pyridin-2-amine (**10**, 8.24 g, 43.3 mmol) and dimethyl sulfide (3.2 g, 52.0 mmol) in DCM (150 mL), *n*-chlorosuccinimide (8.6 g, 65.0 mmol) in DCM (100 mL) was added dropwise over 2 hours while the temperature has maintained at 0 °C. After addition, the mixture was stirred for 2 hours at 0 °C and for an additional 2 hours at

room temperature. A solution of sodium methoxide (4.2 g, 78.0 mmol) in methanol (20 mL) was then added to the mixture. After 15 minutes, water (100 mL) was added to the reaction mixture and stirred overnight at room temperature. After reaction time, the organic layer was separated and the aqueous layer was extracted with DCM. The combined organic layers were dried over MgSO<sub>4</sub>. The solvent was removed by rotovaporation and flash column chromatography was performed using EtOAc as eluent system. The product was obtained in the form of brown oil (6 g, 55%). <sup>1</sup>H NMR (CDCl<sub>3</sub>, 400 MHz): δ 0.17 (s, 9H), 2.76 (s, 6H), 6.57 (d, 1H, *J* = 8.6), 7.36 (d, 1H, *J* = 8.6), 8.08 (s, 1H). <sup>13</sup>C NMR (400 MHz, CDCl<sub>3</sub>): δ -0.3, 32.5, 93.9, 103.1, 107.4, 112.8, 139.4, 150.4, 162.3. HRMS calcd for C<sub>12</sub>H<sub>18</sub>N<sub>2</sub>SSi [M]<sup>+</sup>: 250.0960, found: 250.0967.

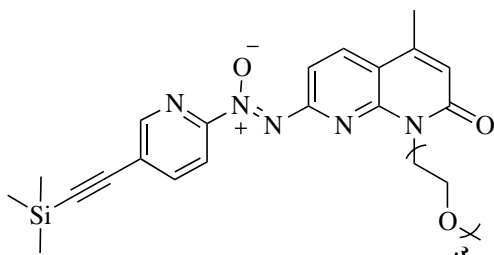
2-Nitroso-5-((trimethylsilyl)ethynyl)pyridine (12).



To 5-((trimethylsilyl)ethynyl)pyridin-2-sulfimine (**11**, 5.5 g, 22.0 mmol) in DCM (20 ml), meta-chloroperoxybenzoic acid (70-75%, 9.2 g, 33.0 mmol) in DCM (50 mL) was added dropwise over 10 minutes while temperature was maintained at 0 °C. After addition, the reaction mixture was stirred for 3 hours at 0 °C. Dimethyl sulfide (1.3 g, 22.0 mmol) was then added to the reaction and the mixture was allowed to warm up to room temperature and stirred for an additional 1 hour. After reaction time, a saturated solution of sodium carbonate was added and the organic layer was separated. The aqueous layer was extracted with DCM (2 x 30 mL). The organic solvent was removed by rotary evaporation at low temperature 20-30 °C to avoid getting more of the dimer molecule affording a brownish solid (3.4 g, 75%) of the monomer and dimer of the title compound **12**. <sup>1</sup>H NMR (CDCl<sub>3</sub>, 400 MHz): δ (monomer) 0.29 (s, 9H), 7.29 (d, 1H, *J* = 8.6), 7.94 (d,

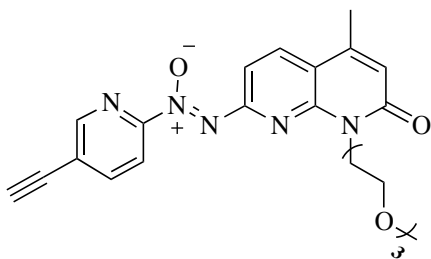
1H,  $J=8.6$ ), 8.82 (s, 1H):  $\delta$  (dimer) 0.25 (s, 9H), 7.79 (d, 1H,  $J=8.6$ ), 8.05 (s, 1H), 8.06 (d, 1H,  $J=8.6$ ).

Acceptor (13).



To (**6**, 4.0 g, 12.4 mmol) and (**12**, 2.5 g, 12.4 mmol) in DCM (100 mL), iodosobenzene diacetate (5.2 g, 16.0 mmol) was added and the reaction mixture stirred overnight under N<sub>2</sub> at 30 °C. After reaction time, the solvent was removed by roto-evaporation. Column chromatography was performed using 4% methanol in DCM as eluent system affording a dark brown oil (2.1 g, 32%). <sup>1</sup>H NMR (CDCl<sub>3</sub>, 400 MHz):  $\delta$  0.26 (s, 9H), 2.43 (s, 3H), 3.28 (s, 3H), 3.42-3.44 (m, 2H), 3.51-3.55 (m, 4H), 3.68 (t, 2H), 3.79 (t, 2H,  $J=6.6$ ), 4.7 (t, 2H,  $J=6.6$ ), 6.6 (s, 1H), 7.88 (d, 1H,  $J=8.2$ ), 8.02 (d, 1H,  $J=8.6$ ), 8.08 (d, 1H,  $J=8.2$ ), 8.33 (d, 1H,  $J=8.6$ ), 8.68 (s, 1H). <sup>13</sup>C NMR (400 MHz, CDCl<sub>3</sub>):  $\delta$  -0.4, 18.2, 58.9, 67.7, 70, 70, 70.2, 70.5, 71.2, 71.7, 71.8, 99.6, 102.9, 112.5, 116.6, 117.2, 122.4, 124.5, 135.1, 142, 144.7, 149, 151.2, 155.3, 162.6. HRMS calcd for C<sub>26</sub>H<sub>33</sub>N<sub>5</sub>O<sub>5</sub>Si [M]<sup>+</sup>: 523.2251, found: 507.2005.

Acceptor (14).



To (**13**, 1.24 g, 2.4 mmol) in dry THF (10 mL), 1 M TBAF (3 mL) was added to the reaction with cooling in an ice bath under N<sub>2</sub>. After addition, the reaction mixture was allowed to stir for 10 minutes at room

temperature. After the reaction, water was added to the mixture and extracted using ethyl acetate. The combined organic layers were dried over sodium sulphate and evaporated under reduced pressure. Flash column was perform for further purification using ethyl acetate as eluent system to afford brown solid (0.8 g, 80%) of the acceptor. <sup>1</sup>H NMR (CDCl<sub>3</sub>, 400 MHz): δ 2.45 (s, 3H), 3.31 (s, 1H), 3.36 (s, 3H), 3.53-3.56 (m, 2H), 3.61-3.67 (m, 4H), 3.74 (t, 2H), 3.82 (t, 2H, *J*=6.6), 4.73 (t, 2H, *J*=6.6), 6.63 (s, 1H), 7.92 (d, 1H, *J*=8.2), 8.08 (d, 1H, *J*=8.6), 8.10 (d, 1H, *J*=8.2), 8.37 (d, 1H, *J*=8.6), 8.75 (s, 1H). <sup>13</sup>C NMR (400 MHz, CDCl<sub>3</sub>): δ 18, 58.7, 67.6, 69.7, 69.8, 70, 70.3 71, 71.5, 71.6, 112.3, 116.4, 117.1, 122.3, 123.3, 134.8, 142.1, 144.4, 148.9, 151.2, 155.1, 155.4, 162.4. HRMS calcd for C<sub>23</sub>H<sub>25</sub>N<sub>5</sub>O<sub>5</sub> [M]<sup>+</sup>: 451.1856, found: 435.18212.

### 4.2.3 Iron Oxide Nanoparticles Synthesis

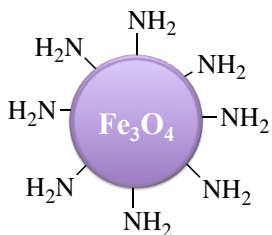
#### Dextran-coated $Fe_3O_4$ nanoparticles (15).



To  $FeCl_3 \cdot 6H_2O$  (0.15g, 0.56 mmol),  $FeCl_2 \cdot 4H_2O$  (0.064g, 0.32 mmol) and dextran (70 K, 1 mL) dissolved in water (2 mL),  $NH_4OH$  (7.5%, 1 mL) was added dropwise over 10 minutes while stirring. This mixture was then warmed to  $70^\circ C$ . After 15 min, the mixture was cooled to room temperature and water (10 mL) was added. The mixture then was centrifuged three times at 4000 rpm for 15 min. Finally, ultrafiltration was performed 6 times to remove excess dextran and reduce the volume.

Iron concentration for nanoparticles **15** = 10.88 mg/mL

#### Cross-linked amine functionalized nanoparticles (16).

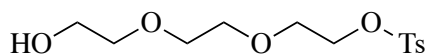


To dextran-coated  $Fe_3O_4$  nanoparticle (4.0 mL, 10.88 mg/mL), NaOH solution (6.54 mL, 5 M) was added under inert atmosphere. After stirring at room temperature for 15 min, Epichlorohydrin (2.67 mL) was then added dropwise to the reaction mixture.. After 8 h,  $NH_4OH$  solution (4 mL, 30%) was added and the mixture was stirred vigorously overnight. Dialysis in a regenerated cellulose membrane (12-14 K) against sodium citrate solution (0.025M) was then performed to remove excess starting materials, followed by ultrafiltration to reduce the volume.

Iron concentration for nanoparticles **16** = 6.49 mg/mL

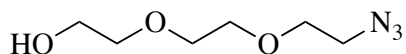
#### 4.2.4 Synthesis of Linker

##### 2-(2-(2-Hydroxyethoxy)ethoxy)ethyl 4-methylbenzenesulfonate (17).



To triethylene glycol (12.0 g, 80.0 mmol), triethylamine (4.0 g, 40.0 mmol) in dichloromethane (100 mL), 4-toluenesulfonyl chloride (3.8 g, 20.0 mmol) was added. The mixture was stirred at room temperature. After 12 hours, the mixture was washed with 1 M potassium bisulfate and 5% sodium bicarbonate and the organic layer was separated and concentrated under reduced pressure providing a colorless oil of the crude product (5.3 g, 22%) which was used for the next reaction without any further purification. <sup>1</sup>H NMR (400 MHz, CDCl<sub>3</sub>): δ 2.27 (s, 3H), 3.29 (s, 1H), 3.38 (t, 2H), 3.41 (s, 4H), 3.52 (t, 4H), 3.99 (t, 2H), 7.20 (d, 2H, *J*=8.2 Hz), 7.62 (d, 2H, *J*=8.2 Hz). <sup>13</sup>C NMR (400 MHz, CDCl<sub>3</sub>): δ 21, 60.9, 67.9, 68.8, 69.5, 70, 72, 127.3, 129.4, 132.2, 144.4. HRMS calcd for C<sub>13</sub>H<sub>20</sub>O<sub>6</sub>S [M]<sup>+</sup>: 304.0981, found: 304.8603.

##### 2-(2-(2-Azidoethoxy)ethoxy)ethanol (18).

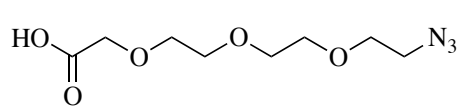


To a solution of 2-(2-(2-hydroxyethoxy)ethoxy)ethyl 4-methylbenzenesulfonate (**17**, 4.0 g, 13.0 mmol) in DMF (50 mL), sodium azide (1.7 g, 26.0 mmol) was added. The mixture was stirred overnight at room temperature. After the reaction time, the mixture was poured into water and extracted with DCM (3 x 50 mL). After washing the organic layer with brine (4 x 100 mL), it was dried over MgSO<sub>4</sub> and solvent was removed under reduced pressure. Flash column chromatography was performed on the crude, using ethyl acetate: Hexane (1:1) as eluent system which afforded a colorless liquid (2.2 g, 97%) of the title



compound.  $^1\text{H}$  NMR ( $\text{CDCl}_3$ , 400 MHz):  $\delta$  3.34 (t, 2H), 3.54 (t, 2H), 3.61-3.63 (m, 6H), 3.65-3.68 (m, 2H).  $^{13}\text{C}$  NMR (400 MHz,  $\text{CDCl}_3$ ):  $\delta$  49.9, 60.6, 69.2, 69.5, 69.8, 72.

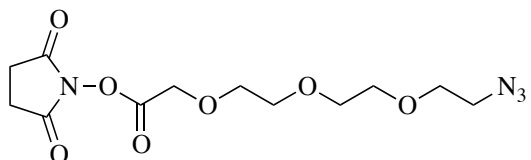
2-(2-(2-(2-Azidoethoxy)ethoxy)ethoxy)acetic acid (19).



2-(2-(2-azidoethoxy)ethoxy)ethanol (**18**, 1.2 g, 7.0 mmol) and bromoacetic acid (0.98 g, 7.0 mmol)

were dissolved in dry THF (20 mL). 60% Sodium hydride (0.78 g, 16.0 mmol) was added under  $\text{N}_2$  and the mixture was refluxed for 24 hours. After the reaction time, the solvent was evaporated and the residue was stirred with 2 M HCl for 3 hours. The mixture was then extracted with dichloromethane (3 x 20 mL). The combined organic layers were dried over  $\text{MgSO}_4$  and evaporated under reduced pressure. Column chromatography using 100% ethyl acetate as eluent system gave a yellowish oil (1.0 g, 62 %).  $^1\text{H}$ -NMR ( $\text{CDCl}_3$ , 400 MHz):  $\delta$  3.38 (t, 2H), 3.64-3.7 (m, 8H), 3.73-3.75 (m, 2H), 4.16 (s, 2H).  $^{13}\text{C}$  NMR (400 MHz,  $\text{CDCl}_3$ ):  $\delta$  50, 67.8, 69.4, 69.9, 70, 70.1, 70.2, 172.5. HRMS calcd for  $\text{C}_8\text{H}_{15}\text{N}_3\text{O}_5$  [ $\text{M}$ ] $^+$ : 234.1012, found: 234.1091.

Water soluble linker (20).



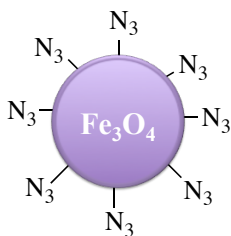
To (**19**, 0.50 g, 2.2 mmol), N-hydroxysuccinimide (0.25 g, 2.2 mmol) and DCC (0.47 g, 2.3 mmol) were added under

inert atmosphere and dissolved in 20 mL of anhydrous acetonitrile. The mixture stirred for 6 hours at 65 °C. After the reaction time, the residue was cooled to room temperature and filtered to remove byproducts and the solvent was evaporated under reduced pressure to afford a colorless oil (0.7 g, 96%) of the corresponding product.  $^1\text{H}$  NMR (400 MHz,

$\text{CDCl}_3$ ):  $\delta$  2.84 (s, 4H), 3.38 (t, 2H), 3.64-3.71 (m, 8H), 3.77-3.79 (m, 2H), 4.51 (s, 2H).

$^{13}\text{C}$  NMR (400 MHz,  $\text{CDCl}_3$ ):  $\delta$  169.2, 166.3, 71.5, 70.8, 70.2, 66.7, 50.9, 25.8.

Conjugation of Linker (20) and Nanoparticles (16), synthesis of nanoparticles (21).



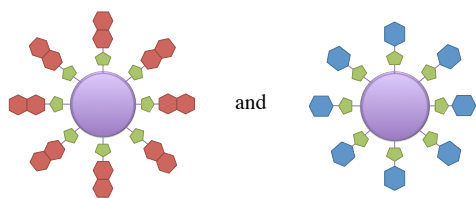
A dialysis was performed against 25 mM pH 7.4 citrate buffer to transfer nanoparticles **16** from pure water to buffer. The linker **20** (16.0 mg, 50.0  $\mu\text{mol}$ ) in 0.25 mL of 1:1 DMSO/  $\text{H}_2\text{O}$  then was added to a solution of nanoparticle **16** (10.0 mg of Fe) in 2.1 mL.

The solution was stirred overnight in the dark. The resulting solution was then dialyzed against pure water for 24 hours to afford nanoparticles **21**.

Iron concentration of nanoparticles **16** after the dialysis = 4.82 mg/mL.

Iron concentration for nanoparticles **21** = 1.83 mg/mL

Conjugation of Donor (3) and Acceptor (14) to Nanoparticle (21), Synthesis of Nanoparticles (22) and (23).



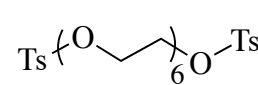
To nanoparticle **17** (1.8 mg of Fe in 1 mL of water) was added the donor, **3** (2.6 mg, 20.0  $\mu\text{mol}$ , 2.0 equivalent per azide) or the acceptor, **14** (8.7 mg, 20.0  $\mu\text{mol}$ , 2.0 equivalent per azide) dissolved in DMF (0.5 mL) under inert atmosphere. Sodium ascorbate (8 mg, 40.0  $\mu\text{mol}$ ) and  $\text{CuSO}_4$  (2.4 mg, 10.0  $\mu\text{mol}$ ) were then added and the mixture was stirred overnight. A dialysis was then performed against 10 mM EDTA, followed by pure water.

Iron concentration of nanoparticles **22** after the dialysis = 1.11 mg/mL.

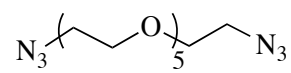
Iron concentration of nanoparticles **23** after the dialysis = 0.58 mg/mL.

#### 4.2.5 Synthesis of the PEG derivative.

##### 3,6,9,12,15-Pentaoxaheptadecane-1,17-diol, 1,17-bis(4-methylbenzenesulfonate) (**24**).

 To hexa(ethylene glycol) (7.0 g, 25.0 mmol) and p-toluenesulfonyl chloride (14.2 g, 75.0 mmol) in dry THF (200 mL), potassium hydroxide (9.3 g, 165.0 mmol) in water (50 mL) was added dropwise over 10 minutes while cooling in an ice bath. After addition, the reaction was stirred under N<sub>2</sub> at room temperature for 36 hours. The solution was then poured into water and neutralized with sulfuric acid and extracted many times with DCM. The combined organic layers were then washed with distilled water and dried over potassium carbonate. The organic layer was evaporated under reduced pressure, and the product was recrystallized from hexane to afford the corresponding product **24** (13.2 g, 90%). <sup>1</sup>H NMR (CDCl<sub>3</sub>, 400 MHz): δ 2.26 (s, 6H), 3.39 (s, 8H), 3.44 (s, 8H), 3.50 (t, 4H, *J*=4.6), 3.98 (t, 4H, *J*=4.6), 7.19 (d, 4H, *J*=8.2), 7.61 (d, 4H, *J*=8.2); <sup>13</sup>C NMR (400 MHz, CDCl<sub>3</sub>): δ 20.9, 67.9, 68.8, 69.9, 127.2, 129.3, 132.3, 144.3. HRMS calcd for C<sub>26</sub>H<sub>38</sub>O<sub>11</sub>S<sub>2</sub> [M]<sup>+</sup>: 590.1856, found: 590.1832.

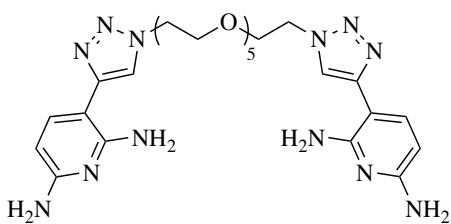
##### 1,17-Diazido-3,6,9,12,15-pentaoxaheptadecane (**25**).

 To (**24**, 12.0 g, 20.0 mmol) in DMF (250 mL), sodium azide (5.3 g, 80.0 mmol) was added. The mixture was stirred for 2 days at room temperature under N<sub>2</sub>. The mixture was then filtered through a thin Celite bed and

the filtrate was poured into a lot of distilled water and extracted many times with chloroform. The combined organic layers were washed (2 x) with distilled water and then dried over MgSO<sub>4</sub>. Solvent was removed by rotary evaporation affording an orange oil (6.68 g, 99%) of the diazide. <sup>1</sup>H NMR (CDCl<sub>3</sub>, 400 MHz): δ 3.24 (t, 4H), 3.51 (s, 8H), 3.52 (s, 8H), 3.53 (t, 4H). <sup>13</sup>C NMR (400 MHz, CDCl<sub>3</sub>): δ 50.1, 69.5, 70.1. HRMS calcd for C<sub>12</sub>H<sub>24</sub>N<sub>6</sub>O<sub>5</sub> [M]<sup>+</sup>: 332.1808, found: 332.1887.

#### 4.2.6 Synthesis of Donor and Acceptor Monomers.

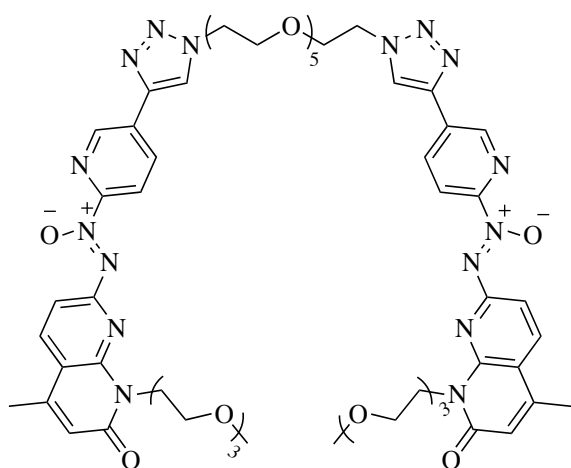
##### Donor Monomer (26).



To 3-ethynylpyridine-2,6-diamine (**3**, 2.0 equivalents, 0.4 g, 3.0 mmol) and 1,17-diazido-3,6,9,12,15-pentaoxaheptadecane (**25**, 1.0 equivalent, 0.49 g, 1.5 mmol) in Toluene (20 mL), CuI (0.65

equivalent, 0.18 g, 0.96 mmol) and DBU (6.5 equivalents, 1.5 g, 9.6 mmol) were added under N<sub>2</sub>. The reaction mixture was stirred for 2 hours under N<sub>2</sub> at 70 °C. The solvent was then removed and the crude product washed with ethyl acetate, CH<sub>2</sub>Cl<sub>2</sub>, and THF affording a brown solid (0.3 g, 33%) of monomer **26**. <sup>1</sup>H NMR (DMSO, 400 MHz): δ 3.42 (s, 4H), 3.45-3.47 (m, 4H), 3.5-3.51 (m, 4H), 3.59 (t, 4H), 3.83 (t, 4H), 4.51 (t, 4H), 5.67 (s, 4H), 5.77 (d, 2H, *J*=8.2), 6.49 (s, 4H), 7.45 (d, 2H, *J*=8.2), 8.25 (s, 2H). HRMS calcd for C<sub>26</sub>H<sub>38</sub>N<sub>12</sub>O<sub>5</sub> [M]<sup>+</sup>: 598.3088, found: 598.3109.

Acceptor Monomer (27).



To of (E)-7-((5-ethynylpyridin-2-yl)diazenyl)-2-(2-(2-(2-methoxyethoxy)ethoxy)ethoxy)-4-methyl-1,8-naphthyridine (**14**, 2.0 equivalents, 0.5 g, 12.0 mmol) and 1,17-diazo-3,6,9,12,15-pentaoxaheptadecane (**25**, 1.0 equivalent, 0.2 g, 0.6 mmol) in Toluene (20 mL), CuI ( 0.65 equivalent, 0.075 g, 0.39

mmol) and DBU (6.5 equivalents, 0.6 g, 3.9 mmol) were added under nitrogen. The reaction mixture stirred for 2 hours under N<sub>2</sub> at 70 °C. After reaction time, the solvent was concentrated using reduced pressure and the resulting crude was dissolved in DCM and washed with a saturated aqueous solution of EDTA and then water. The organic layer was dried over MgSO<sub>4</sub> and evaporated affording yellowish oil (0.1 g, 14%) of monomer **27**. <sup>1</sup>H NMR (CDCl<sub>3</sub>, 400 MHz): δ 2.46 (s, 6H), 3.31 (s, 6H), 3.45-3.48 (m, 4H), 3.54-3.58 (m, 8H), 3.6-3.65 (m, 16H), 3.71 (t, 4H), 3.83 (t, 4H), 3.94 (t, 4H), 4.65 (t, 4H), 4.75 (t, 4H), 6.63 (s, 2H), 7.92 (d, 2H, *J*=8.2), 8.11 (d, 2H, *J*=8.2), 8.34 (s, 2H), 8.46 (d, 2H, *J*=8.6), 8.55 (d, 2H, *J*=8.6), 9.10 (s, 2H). <sup>13</sup>C NMR (400 MHz, CDCl<sub>3</sub>): δ 18.2, 50.5, 58.9, 67.8, 69.2, 69.9, 70, 70.4, 70.45, 70.5, 70.54, 70.6, 71.8, 112.5, 116.5, 116.7, 118, 122.5, 122.8, 130.8, 131.1, 134.9, 135.8, 142.8, 144.5, 145.5, 149.2, 162.6.

## **Chapter 5: References**

- 1) Zimmerman, S. C.; Corbin, p. S. *In structure and bonding*; Springer Verlag Berlin Heidelberg: **2000**; Vol. 96.
- 2) Rehm, T.; Schmuck, C. *Chem. Commun.* **2008**, 7, 801.
- 3) Fenske, T.; Korth, H.-G.; Mohr, A.; Schmuck, C. *Chem.--Eur. J.* **2012**, 18, 738.
- 4) Schneider, H. J.; Juneva, R. K.; Simova, S. *Chem. Ber.* **1989**, 122, 1211.
- 5) Wilson, A. J. *Soft Matter*, **2007**, 3, 409.
- 6) Jorgensen, W. L.; Pranata, J. *J. Am. Chem. Soc.* **1990**, 112, 2008.
- 7) Djurdjevic, S.; Leigh, D. A.; McNab, H.; Parsons, S.; Teobaldi, G.; Zerbetto, F. *J. Am. Chem. Soc.* **2006**, 129, 476.
- 8) Blight, B. A.; Hunter, C. A.; Leigh, D. A.; McNab, H.; Thomson, P. I. T. *Nat Chem* **2011**, 3, 244.
- 9) Kyogoku, Y., Lord, R.C., Rich, A. *Proc. Natl. Acad. Sci. U. S. A.* **1967**, 57, 250.
- 10) Blight, B. A.; Camara-Campos, A.; Djurdjevic, S.; Kaller, M.; Leigh, D. A.; McMillan, F. M.; McNab, H.; Slawin, A. M. Z. *J. Am. Chem. Soc.* **2009**, 131, 14116.
- 11) Cook, J. L.; Hunter, C. A.; Low, C. M. R.; Perez-Velasco, A.; Vinter, J. G. *Angew. Chem., Int. Ed.* **2007**, 46, 3706.
- 12) Mudraboyina, B. P.; H.-B., W.; Newbury, R.; Wisner, J. A. *Acta Cryst.* **2011**, E67.
- 13) Peng, X.-H.; Qian, X.; Mao, H.; Wang, A. Y.; Chen, Z. G.; Nie, S.; Shin, D. M. *Int. J. Nanomedicine.* **2008**, 3, 311.
- 14) Karve, S.; Bandekar, A.; Ali, M. R.; Sofou, S. *Biomaterials.* **2010**, 31, 4409.
- 15) Lodhia, J.; Mandarano1, G.; Ferris, N.; Eu, P.; Cowell, S. *Biomed Imaging Interv J.* **2010**, 6.
- 16) Gribouski, E. Qualifying Project, *Worcester Polytechnic Institute*, **2009**.

- 17) Lauffer, R. B. *Chem. Rev.* **1987**, *87*, 901.
- 18) Qiao, R.; Yang, C.; Gao, M. *J. Mater. Chem.* **2009**, *19*, 6274.
- 19) Martin, A. L.; Bernas, L. M.; Rutt, B. K.; Foster, P. J.; Gillies, E. R. *Bioconjugate Chem.* **2008**, *19*, 2375.
- 20) Villaraza, A. J.; Bumb, A.; Brechbiel, M. W. *Chem. Rev.* **2010**, *110*, 2921.
- 21) Qiao, R.; Yang, C.; Gao, M. *J. Mater. Chem.* **2009**, *19*, 6274.
- 22) Veiseh, O.; Sun, C.; Gunn, J.; Kohler, N.; Gabikian, P.; Lee, D.; Bhattarai, N.; Ellenbogen, R.; Sze, R.; Hallahan, A.; Olson, J.; Zhang, M. *Nano Letters.* **2005**, *5*, 1003.
- 23) Serda, R. E.; Adolphi, N. L.; Bisoffi, M. *Mol. Imaging.* **2007**, *6*, 277.
- 24) Sun, C.; Sze, R.; Zhang, M. *J. Biomed. Mater. Res., Part A.* **2006**, *78*, 5507.
- 25) Perez, J. M.; Simeone, F. J.; Saeki, Y.; Josephson, L.; Weissleder, R. *J. Am. Chem. Soc.* **2003**, *125*, 10192.
- 26) Bagal, S. K.; Gibson, K. R.; Kemp, M. I.; Poinard, C.; Stammen, B. L.; Denton, S. M.; Glossop, M. S. *In Canadian Intellectual Property Office Canada*, WO **2008/135826 A3**.
- 27) Elangovan, A.; Wang, Y.-H.; Ho, T.-I. *Org. Lett.* **2003**, *5*, 1841.
- 28) Aakeroy, C. B.; Schultheiss, N.; Desper, J. *Dalton Trans.* **2006**, *13*, 1627.
- 29) Leonard, J. T.; Gangadhar, R.; Gnanasam, S. K.; Ramachandran, S.; Saravanan, M.; Sridhar, S. K. *Biol. Pharm. Bull.* **2002**, *25*, 798.
- 30) Santos, M. A. I.; Afonso, A.; Marques, M. M.; Wilcox, C. *Supramol. Chem.* **2000**, *11*, 201.
- 31) Snow, A. W.; Foos, E. E. *Synthesis.* **2003**, 509.



- 32) Li, H.; Jensen, T. J.; Fronczek, F. R.; Vicente, M. G. a. H. J. *Med. Chem.* **2008**, *51*, 502.
- 33) Kumar, K. K.; Elango, M.; Subramanian, V.; Das, T. M. *New J. Chem.* **2009**, *33*, 1570.
- 34) Schneider, S.; Kessler, D., Veen, L., Wunberg, T. *Patent Application Publication*, US **2012/0028958** A1.
- 35) Taylor, E. C.; Tseng, C. P.; Rampal, J. B. *J. Org. Chem.* **1982**, *47*, 552.
- 36) Li, F.; Yang, B.; Miller, M. J.; Zajicek, J.; Noll, B. C. *Org. Lett.* **2007**, *9*, 2923.
- 37) Gowenlock, B. G.; Maidment, M. J.; Orrell, K. G.; Sik, V.; Mele, G.; Vasapollo, G.; Hursthouse, M. B. *J. Am. Chem. Soc., Perkin Transactions 2.* **2000**, *11*, 2280.
- 38) Boschi, D.; Guglielmo, S.; Aiello, S.; Morace, G.; Borghi, E.; Fruttero, R. *Med. Chem. Lett.* **2011**, *21*, 3431.
- 39) Matsukura, M. I., S; Murai, N.; Shirotori, S. *Patent Application Publication*, US 2010/0099718 A1.
- 40) Molday, R. S.; Mackenzie, D. *J. Immunol. Methods.* **1982**, *52*, 353.
- 41) Pittet, M. J.; Swirski, F. K.; Reynolds, F.; Josephson, L.; Weissleder, R. *Nat. Protocols* **2006**, *1*, 73.
- 42) Ameijde, J. v.; Liskamp, R. M. J. *Org. Biomol. Chem.* **2003**, *1*, 2661.
- 43) Schmidt, F.; Rosnizeck, I. C.; Spoerner, M.; Kalbitzer, H. R. *Inorg. Chim. Acta.* **2011**, *365*, 38.
- 44) Gong, Y.; Luo, Y.; Bong, D. *J. Am. Chem. Soc.* **2006**, *128*, 14430. Linker synthesei
- 45) Gothard, C. M.; Grzybowski, B. A. *Synthesis.* **2012**, *5*, 717.

- 46) LaFrate, A. L.; Carlson, K. E.; Katzenellenbogen, J. A. *Bioorg. Med. Chem.* **2009**, *17*, 3528.
- 47) Hua, Y.; Flood, A. H. *J. Am. Chem. Soc.* **2010**, *132*, 12838.
- 48) Iranpoor, N.; Firouzabadi, H.; Khalili, D. *Bull. Chem. Soc. Jpn.* **2010**, *83*, 923.
- 49) Kucharska, E.; Hanuza, J.; Talik, Z. *Chem. Phys.* **2004**, *306*, 71.
- 50) Gan, X.; Chi, S.-M.; Mu, W.-H.; Yao, J.-C.; Quan, L.; Li, C.; Bian, Z.-Y.; Chen, Y. *Dalton Trans.* **2011**, *40*, 7365.
- 51) Drewry, J. A.; Fletcher, S.; Hassan, H.; Gunning, P. T. *Org. Biomol. Chem.* **2009**, *7*, 5074.

## Curriculum Vitae: Fatimah Algarni

### EDUCATION:

**2003-2007** Girls College of Education / Scientific Sections, King Abdulaziz University, Jeddah, Mecaa, SAUDI ARABIA, B.Sc. (Honors Chemistry)

**2010-till** present date University of Western Ontario, London, Ontario, CANADA, Graduate Program

### ACADEMIC POSITIONS:

**2007-2009** – Demonstrator/Teaching Assistant at Department of Chemistry, Faculty of Science, King Abdulaziz University, Saudi Arabia.

### GRADUATE LEVEL COURSES COMPLETED:

MECHANISTIC ORGANIC CHEMISTRY Grade: 84

NANOBIOTECHNOLOGY Grade: 85

CHEMISRT SEMINAR Grade: 81

### PRESENTATIONS:

Algarni, F. M.; Wisner, G. A.; Gillies, E. R. "The Hydrogen-bonded Complex of 2,6-Diaminopyridinium Cation with an Azonaphthyridine." *Summer School in Supramolecular Chemistry*, Montreal, Canada, June 10, **2011**. Oral.